Conceptual models for short-eccentricity-scale climate control on peat formation in a lower Palaeocene fluvial system, north-eastern Montana (USA)

Noorbergen, Lars J.; Abels, Hemmo A.; Hilgen, Frederik J.; Robson, Brittany E.; de Jong, Edwin; Dekkers, Mark J.; Krijgsman, Wout; Smit, Jan; Collinson, Margaret E.; Kuiper, Klaudia F.

DOI
10.1111/sed.12405

Publication date
2017

Document Version
Final published version

Published in
Sedimentology

SEDIMENTOLOGY the journal of the International Association of Sedimentologists

Sedimentology (2017) doi: 10.1111/sed.12405

Conceptual models for short-eccentricity-scale climate control on peat formation in a lower Palaeocene fluvial system, north-eastern Montana (USA)

LARS J. NOORBERGEN*, HEMMO A. ABELS†, FREDERIK J. HILGEN‡, BRITTANY E. ROBSON§, EDWIN DE JONG‡, MARK J. DEKKERS‡, WOUT KRIJGSMAN‡, JAN SMIT*, MARGARET E. COLLINSON§ and KLAUDIA F. KUIPER*

**Department of Earth Sciences, VU University Amsterdam, De Boelelaan 1085, 1081 HV, Amsterdam, The Netherlands (E-mail: l.j.noorbergen@gmail.com)*

†Department of Geosciences and Engineering, Delft University of Technology, Stevinweg 1, 2628 CN, Delft, The Netherlands

‡Department of Earth Sciences, Utrecht University, Budapestaan 4, 3584 CD, Utrecht, The Netherlands

§Department of Earth Sciences, Royal Holloway University of London, Egham, Surrey, TW20 0EX, UK

Associate Editor – Christopher Fielding

ABSTRACT

Fluvial systems in which peat formation occurs are typified by autogenic processes such as river meandering, crevasse splaying and channel avulsion. Nevertheless, autogenic processes cannot satisfactorily explain the repetitive nature and lateral continuity of many coal seams (compacted peats). The fluvial lower Palaeocene Tullock Member of the Fort Union Formation (Western Interior Williston Basin; Montana, USA) contains lignite rank coal seams that are traceable over distances of several kilometres. This sequence is used to test the hypothesis that peat formation in the fluvial system was controlled by orbitally forced climate change interacting with autogenic processes. Major successions are documented with an average thickness of 6·8 m consisting of *ca* 6 m thick intervals of channel and overbank deposits overlain by *ca* 1 m thick coal seam units. These major coal seams locally split and merge. Time-stratigraphic correlation, using a Cretaceous–Palaeogene boundary event horizon, several distinctive volcanic ash-fall layers, and the C29r/C29n magnetic polarity reversal, shows consistent lateral recurrence of seven successive major successions along a 10 km wide fence panel perpendicular to east/south-east palaeo-flow. The stratigraphic pattern, complemented by stratigraphic age control and cyclostratigraphic tests, suggests that the major peat-forming phases, resulting in major coal seams, were driven by 100 kyr eccentricity-related climate cycles. Two distinct conceptual models were developed, both based on the hypothesis that the major peat-forming phases ended when enhanced seasonal contrast, at times of minimum precession during increasing eccentricity, intensified mire degradation and flooding. In model 1, orbitally forced climate change controls the timing of peat compaction, leading to enhancement of autogenic channel avulsions. In model 2, orbitally forced climate change controls upstream sediment supply and clastic influx determining the persistence of peat-forming conditions. At the scale of the major successions, model 2 is supported because interfingering channel sandstones do not interrupt lateral continuity of major coal seams.

Keywords Conceptual model, fluvial system, lignite rank coal, north-eastern Montana, orbitally forced climate change, Palaeocene, peat formation, time-stratigraphic correlation.

INTRODUCTION

The repetitive nature and lateral continuity of coal seams in fluvial stratigraphic architectures have long been recognized in outcrops and the subsurface (e.g. Wanless & Weller, 1932; Cecil, 1990; Fielding & Webb, 1996; Paproth *et al.*, 1996; Michaelsen & Henderson, 2000). Such features of coal seams in fluvial successions may reflect recurrent phases of peat formation through time over wide areas, that may point to orbital-scale climate control on peat formation in the fluvial system. However, there is little previous research investigating possible relationships between peat formation in fluvial systems and orbitally forced climate changes. Geographically widespread peat formation is mostly documented in deltaic settings during rising groundwater levels (e.g. Aitken & Flint, 1995) and may be linked to orbital-scale climate control on sea-level change (e.g. Heckel, 2008). However, with rising sea-level as a primary control on orbital timescales, peat formation develops diachronously through time along the direction of transgression (e.g. Bohacs & Suter, 1997). In fluvial settings that are not (or are less) influenced by sea-level changes on orbital timescales, but are primarily allogenically controlled by orbital-scale climate control on river discharge and sediment supply, peat formation may be synchronous over a wide area (e.g. Fielding & Webb, 1996). Fielding & Webb (1996) argued for precession-scale climate control on peat formation in a fluvial system, based on a sedimentological analysis of the late Permian Bainmedart coal measures in Antarctica. Spectral analysis of a lithology record was used to test for this climate control. This showed two main peaks at 10·5 m and 19·0 m with a 1·8 ratio, that is close to the ratio of the 19 kyr period of precession and 35 kyr period of obliquity in the Permian. The 19 kyr cycle durations summed to an estimated time duration of 2·1 to 2·3 Myr for the Bainmedart coal measures, which is within the range of palynostratigraphic age estimations of <3·3 Myr.

Isolating orbitally forced climate change from autogenic processes is essential for a better understanding of fluvial sedimentation and predicting changes in river environments (Abels *et al.*, 2013). Also, it has been hypothesized that periodic storage of atmospheric CO_2 on orbital timescales, in vast peat-producing continental basins in North America and Eurasia, played a significant role in global carbon cycling in the Late Palaeocene and Early Eocene (Zachos *et al.*, 2010). However, in the stratigraphic architecture of coal-bearing fluvial deposits, orbitally forced climate changes (10 kyr to 1 Myr) are difficult to disentangle from other time-overlapping controls taking place outside (allogenic) or inside (autogenic) the fluvial system. For instance, allogenic control by tectonic-scale changes in basin subsidence (100 kyr to 10 Myr) can be substantial. Examples of time-overlapping autogenic processes are stream avulsion (1 to 10 kyr) and point-bar migration (100 to 1000 year). These autogenic processes cause lateral heterogeneity in sedimentation at variable rates. Such heterogeneity obscures the imprint of more regional-scale processes, such as variations in discharge, that might be caused by orbitally forced changes in precipitation. The autogenic avulsion model is widely adopted in studies on coal-bearing fluvial successions. It considers differential peat compaction as a major autogenic control on channel avulsion resulting in diagonally stacked channel sandstones over time (e.g. Fielding, 1984). However, in many cases, the repetitive nature and lateral continuity of coal seams observed in the geological record of fluvial deposits suggest that possible control by orbitally forced climate change should also be taken into account (e.g. Fielding & Webb, 1996). That there is little previous research investigating this relationship may be a consequence of independent dating methods being relatively scarce in fluvial deposits, often precluding the integration of time into a depositional model. A coal-bearing fluvial succession that is potentially very suitable for a combination of sedimentology, cyclostratigraphy and geochronology is the Tullock Member of the Fort Union Formation in the Western Interior Williston Basin (Montana, USA). It is well-exposed in the Badlands along the Missouri River of north-eastern Montana.

Lignite rank coal zones in the lower part of the Tullock Member have been traced over distances of several kilometres in separate outcrop areas in McCone County (Collier & Knechtel, 1939). However, an allogenic depositional model was never suggested in previous studies. Long distance, kilometre-scale correlations are difficult to prove due to lateral complexity, with coal seams laterally splitting into multiple thinner beds. Also, local outcrop areas are often exposed in buttes and ridges separated from one another by later erosion. Therefore, regional correlations must be accomplished by other techniques such as detailed sedimentological comparisons, distinctive time-stratigraphic marker beds and magnetostratigraphy. The uppermost Hell Creek Formation and the Tullock Member in north-eastern Montana contain several time-stratigraphic markers. These include the Cretaceous–Palaeogene boundary (KPB) impact claystone (Alvarez, 1983; Bohor *et al.*, 1984; Smit & van der Kaars, 1984; Baadsgaard *et al.*, 1988; Moore *et al.*, 2014), the C29r/C29n magnetic polarity reversal boundary (Swisher *et al.*, 1993; LeCain *et al.*, 2014) and numerous zircon-bearing and sanidine-bearing volcanic ash-fall layers (tephras), generally preserved within the coal seams and suitable for $^{40}Ar/^{39}Ar$ radio-isotope dating (Swisher *et al.*, 1993; Renne *et al.*, 2013; Sprain *et al.*, 2015), U-Pb radio-isotope dating (Renne *et al.*, 2013) and geochemical fingerprinting (Ickert *et al.*, 2015).

In this study, a multi-disciplinary approach is used to understand the origin of the coal repetitions along a *ca* 10 km wide NNE–SSW transect of the Tullock Member in north-eastern Montana consisting of 13 sections. Coal petrographic analysis was used to understand aspects of the peat-forming environment and to identify inertinite (i.e. charcoal) in the lignites and hence document the occurrence of fires. Lateral continuity of coal seams along the transect was tested using tephrastratigraphic and magnetostratigraphic correlations. The resulting stratigraphic fence panel was used to provide a quantitative assessment of main lithofacies thickness, and thereby to test for the lateral significance of frequencies revealed from spectral analyses of local overbank records. In order to filter significant frequencies from the overbank records, a coal decompaction ratio has been applied to account for the impact of peat compaction on stratigraphic thicknesses. The results are synthesized in two conceptual models for orbital-scale climate control on peat formation in this early Palaeocene fluvial system.

GEOLOGICAL SETTING

The Western Interior Williston Basin

The Williston Basin is an intracratonic depocentre that became part of the Western Interior Foreland Basin during the Cretaceous (DeCelles, 2004). Between the Middle Albian (*ca* 110 Ma) and Early Maastrichtian (*ca* 70 Ma), marine sedimentation dominated in the Western Interior Seaway including widespread deposition of marine shales (DeCelles, 2004). During Laramide uplift in the Late Maastrichtian, an eastward prograding fluvio-deltaic system developed, depositing mainly fine-grained sediments that belong to the Hell Creek Formation in north-eastern Montana (Cherven & Jacob, 1985). The delta progradation led to regression of the Western Interior Seaway and possible disconnection by a tidal flat area in the Dakotas, the so-called 'Dakota Isthmus', separating a northern remnant connected with the Arctic Ocean and a southern remnant connected with the Gulf of Mexico (Erickson, 1999; Hartman *et al.*, 2014), i.e. the origin of the Cannonball Sea(s). In the Western Interior Williston Basin, the lithostratigraphy across the KPB (Cretaceous–Palaeogene boundary) is characterized by a marked change. The light-grey-greenish, somber-weathered beds of the upper Cretaceous Hell Creek Formation are overlain by coal-bearing, typically thin-banded, grey-gold-brownish beds of the lower Palaeocene Tullock Member (Fig. 2) of the Fort Union Formation (e.g. Rigby & Rigby, 1990). This lithological change has been attributed to either gradual ponding or catastrophic flooding of the palaeolandscape subsequent to the KPB (Fastovsky & Bercovici, 2016). Gradual ponding has been suggested to be a consequence of elevated water tables resulting from either: (i) increased rainfall (Fastovsky, 1987); or (ii) Danian sea-level rise of the Cannonball Sea(s) (Sloan & Rigby, 1986). Fastovsky & Bercovici (2016) suggested that catastrophic flooding could be a consequence of landscape denudation as a result of wildfire-induced deforestation caused by the heat pulse and fallout of the Chicxulub meteorite impact. Fastovsky & Bercovici (2016) cited various literature supporting the scenario of wildfire-induced deforestation but did not consider work by Belcher *et al.* (2009) in which multiple sources of evidence failed to support that scenario. Subsequent to the KPB, peat-forming environments in the Western Interior Williston Basin seem to gradually change from low-lying mires

(Fastovsky, 1987; Jerrett *et al.*, 2015) to raised mires (Flores & Keighin, 1999; Flores *et al.*, 1999).

The Tullock Member (Palaeocene) in north-eastern Montana

In north-eastern Montana, the Lower Palaeocene Tullock Member consists of several coal seams alternating with siliciclastic sediments (Collier & Knechtel, 1939; Rigby & Rigby, 1990). The alternations between coal beds and thinly banded siltstones form excellent lithological criteria to distinguish the Tullock Member from the grey, somber-weathered mudstones of the underlying Hell Creek Formation (Fig. 2A and H) and the coal-bearing dark-grey shales of the overlying Lebo Shale Member. Coal seams of the Tullock Member formed in low-lying mires dissected by meandering rivers (Fastovsky & Dott, 1986; Fastovsky, 1987; Fastovsky & Bercovici, 2016) that drained towards the Cannonball Sea(s) (Cherven & Jacob, 1985). Thinly banded siltstones (Fig. 2D) may have formed in extensive, low-energy, ponded water environments dissected by small feeder channels (Fastovsky, 1987). The siltstones are interpreted as recording the precursory phase of lacustrine and marshy conditions in nearly filled, local floodbasins (Rigby & Rigby, 1990). These beds have also been termed 'variegated beds' (Archibald, 1982) or 'zebra-striped beds' (Rigby & Rigby, 1990). Palaeosols in the Tullock Member generally are weakly developed, mostly are histosols, and probably formed in humid climates although dry periods also existed in the mires indicated by deeply penetrating root traces, slicken-sided claystone and features of chemical weathering below the coal seams (Retallack, 1994). In addition, the presence of charcoal in most carbonaceous shale and coal beds indicates occurrences of wildfires (Rigby & Rigby, 1990). Volcanic ash-fall layers are mainly observed in coal beds, probably owing to the higher preservation potential in low-energy peat-forming mires (e.g. Sprain *et al.*, 2015). The igneous source of the tephras may be the Idaho and Boulder batholiths (Ickert *et al.*, 2015).

Coal nomenclature of the Tullock Member in McCone County

Collier & Knechtel (1939) introduced a reversed alphabetic nomenclature (from Z to P) for coal zones of the lower Fort Union Formation in McCone County. Coal zones are half a metre to a few metres thick and often consist of thin clastic partings (for example, sandstones, siltstones or carbonaceous shales) separating coal beds of generally 0·2 to 0·3 m thickness (Rigby & Rigby, 1990). The Z-coal is the first coal zone above the last *in situ* preserved dinosaur remains (Rigby & Rigby, 1990). In McCone County, it has been subdivided by Rigby & Rigby (1990) into an event-Z-coal and a Formational Z (FmZ)-coal (MCZ in Lofgren *et al.*, 1990; Lofgren, 1995). The event-Z-coal occurs in the uppermost part of the Hell Creek Formation. Rarely preserved at the very base of the event-Z-coal, a *ca* <1 cm thick impact-ejecta layer occurs, enriched in iridium, i.e. associated with the catastrophic Chicxulub meteorite impact held responsible for extinctions at the KPB (Alvarez *et al.*, 1980; Smit & Hertogen, 1980; Smit & Klaver, 1981). The event-Z-coal is laterally discontinuous and can be replaced laterally by a carbonaceous shale. In McCone County, microtektite-like spherules or shocked minerals have never been recognized in the stratigraphic interval of the KPB. The presence of the event-Z-coal has been suggested at Bug Creek (BCM in Fig. 1) where a slight enrichment of Iridium (two to three times background) was found at the base of a carbonaceous shale, *ca* 1·5 m below the base of the FmZ-coal (Sloan *et al.*, 1986; Fastovsky & Dott, 1986). A change from Cretaceous to Palaeocene pollen at the same stratigraphic level (Rigby *et al.*, 1987; Smit *et al.*, 1987) supports this position of the KPB at Bug Creek. In contrast to the event-Z-coal, the FmZ-coal is a prominent continuous coal, frequently marking the lithostratigraphic boundary between light-grey-greenish beds of the Hell Creek Formation and grey-gold-brownish beds of the overlying Tullock Member (Rigby & Rigby, 1990).

The interval studied here encompasses the Z, Y, X and W-coal zones (Collier & Knechtel, 1939; Rigby & Rigby, 1990). Within the succession of these four coal zones, eight distinct and persistent coal seams were identified and assigned numerical labels, in stratigraphic order. To show the connection with the reversed alphabetic nomenclature of the coal zones, the alphabetic letter system is retained in the refined labelling of the coal seams. The #1-Z-coal now refers to the lowest coal seam (number 1) of the Tullock Member at the base of the Z-coal zone. The #2-Z-coal is stratigraphically the second coal seam of the Tullock Member, above #1-Z, at the top of the Z-coal zone. The #3-Y-coal is the third coal seam, and in this particular

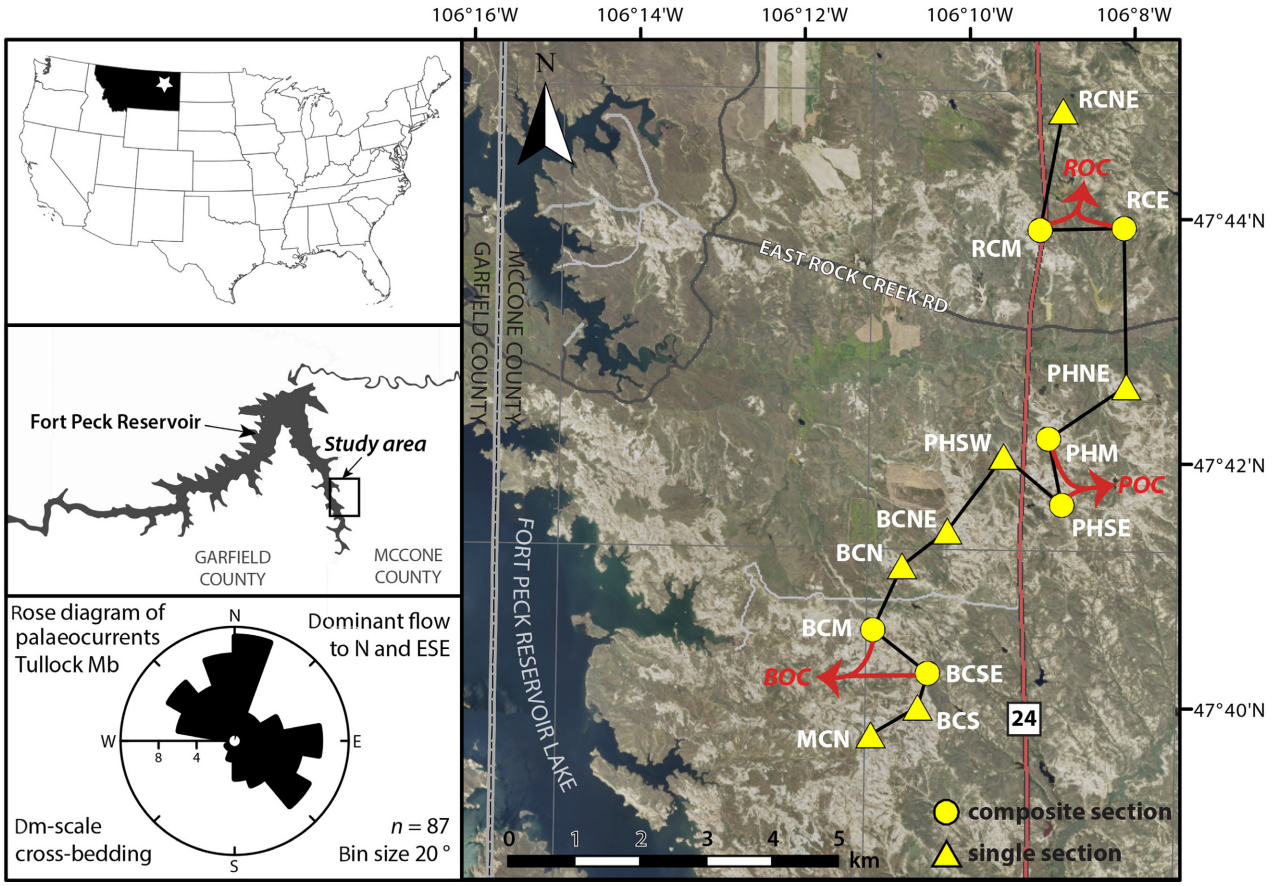

Fig. 1. Geographic setting of the study area in McCone County, north-eastern Montana (USA). The locations of the composite sections (yellow circles) and single sections (yellow triangles) are connected along a transect (solid line). The Rock Creek, Purgatory Hill and Bug Creek overbank composites (respectively, ROC, POC and BOC) are indicated by the red brackets. In the bottom left, a rose diagram shows palaeocurrent data of the Tullock Member measured on decimetre-scale cross-bedded channel sandstones. Two dominant flow directions are observed, towards the north and ESE; the latter being perpendicular to the orientation of the transect. A fence panel of the two-dimensional transect is shown in Fig. 6. Orthoimagery, quadrangle and road data were obtained from the Montana Spatial Data Infrastructure (MSDI) (http://geoinfo.msl.mt.gov/Home/msdi). Abbreviations (from north to south): RCNE, Rock Creek North-east; RCM, Rock Creek Main; RCE, Rock Creek East; PHNE, Purgatory Hill North-east; PHM, Purgatory Hill Main; PHSE, Purgatory Hill South-east; PHSW, Purgatory Hill South-west; BCNE, Bug Creek North-east; BCN, Bug Creek North; BCM, Bug Creek Main; BCSE, Bug Creek South-east; BCS, Bug Creek South; MCN, McGuire Creek North.

case is equivalent to the Y-coal zone of Collier & Knechtel (1939) and Rigby & Rigby (1990). Above coal #3-Y, coal seams #4-X, #5-X, #6-X, #7-W and #8-W are identified. These coal seams can be correlated to outcrops of the Tullock Member adjacent to the study area (Fig. 1). Longer distance correlations between isolated outcrop areas (for instance the outcrops of the Tullock Member in McCone and Garfield Counties) are more complicated because changes in the rate of sedimentation and accommodation that prevailed in the peat-forming environment might have resulted in splitting and merging of coal seams causing thickness variations up to tens of metres.

Lithostratigraphic boundaries

The Hell Creek–Tullock lithostratigraphic boundary has been defined at the base of the first coal zone above the last *in situ* preserved dinosaur remains (Brown, 1952). This definition was recently refined with the formational boundary placed either at the base of the stratigraphically lowest coal layer, or at the base of the laminated silt-rich flood deposits referred to as variegated

beds (Fastovsky & Bercovici, 2016). These grey-gold-brownish, thinly banded beds are highly distinctive for the Tullock Member. Laterally, extensive coal seams are prominent but in themselves are not diagnostic as a lithostratigraphic criterion since such coal seams can also be present in the Hell Creek Formation such as the Null-coal (Smit *et al.*, 1987). Also, the lowest variegated beds can pass laterally into a coal seam (Fastovsky & Bercovici, 2016). In that case, the coal layer forms the lithostratigraphic boundary between the light-grey-greenish, somber-weathered beds of the Hell Creek Formation and the grey-gold-brownish, thinly banded beds of the Tullock Member. The lithostratigraphic boundary, either defined by the base of the lowest variegated beds or the base of the FmZ-coal (Fastovsky & Bercovici, 2016), is therefore considered most appropriate and is used here (Fig. 2A and E to H).

The Tullock–Lebo Shale lithostratigraphic boundary is commonly placed at the base of a thick, widespread coal bed that contains many volcanic ash layers (Thom & Dobbin, 1924) named the Big Dirty coal zone (Woolsey *et al.*, 1917). In McCone County, the Tullock–Lebo Shale boundary is defined at the base of the U-coal zone, supposedly correlative to Big Dirty (Collier & Knechtel, 1939). The base of the U-coal for the Tullock–Lebo Shale boundary was used for mapping purposes (Collier & Knechtel, 1939) but is not in itself diagnostic since Lebo Shale-type dark-grey, somber-weathered shale units were also recognized below the U-coal, almost down to just above the W-coal zone (Rigby & Rigby, 1990). Moreover, the stratigraphic position of the Big Dirty coal zone in the Bull Mountain coal field (central Montana), where this zone was originally defined, is in the middle part of the Lebo Shale Member (Woolsey *et al.*, 1917). Therefore, the U-coal zone is not ideal as a lithostratigraphic boundary criterion for the Tullock–Lebo Shale boundary. In this study, the transition from thinly banded siltstones to dark-grey, somber-weathered shales is used as the boundary between the Tullock and Lebo Shale Members (Fig. 2F).

METHODS

Sections and fieldwork

The study area is located in McCone County, east of Fort Peck Reservoir of the Missouri River, where six composite sections and seven single sections were investigated (Fig. 1). The composite sections are located in the areas of Bug Creek (e.g. Fastovsky & Dott, 1986; Retallack, 1994), Purgatory Hill (e.g. Sloan & Van Valen, 1965; Swisher *et al.*, 1993) and Rock Creek (Rigby & Rigby, 1990). In these areas, a main section was logged from a few centimetres to metres below the Hell Creek–Tullock lithostratigraphic boundary. At approximately 0·5 to 1·0 km distance from the main section, partly overlapping sections were logged to include younger strata. The composite sections in the same outcrop area were merged into single overbank composites, using a distinctive tephra horizon in the overlapping interval for correlation (Figs 8 and S1). The three overbank composites are the Rock Creek Overbank Composite (ROC), the Purgatory Hill Overbank Composite (POC) and the Bug Creek Overbank Composite (BOC) (Fig. 1). Note that composite sections were constructed exclusively using the overbank successions. Thus,

Fig. 2. Field photographs. (A) Coal-clastic alternations in the Tullock Member (Mb) at Bug Creek Main. The approximate position of the KPB (Cretaceous–Palaeogene boundary) is at the base of a coaly layer in the uppermost part of the Hell Creek Formation (Fm). (B) Splitting of major coal #3-Y into two minor coals at Purgatory Hill North-east. White dashed line shows logged transect of a single section. (C) Tullock Member at Purgatory Hill Main and view towards north showing Highway 24 and locations of Rock Creek sections. (D) A 3 m thick interval of thinly banded siltstones that typify floodplain successions in the Tullock Member, Purgatory Hill. (E) Relatively small channel fill complex in the Z-coal zone in between #1-Z and #2-Z. Coal #1-Z is not eroded by the overlying sandstone. Bug Creek. (F) The Tullock Member at McGuire Creek North underlain and overlain by the Hell Creek Formation and the Lebo Shale Member, respectively. Above the Y-coal and above the X-coal zones, 12 to 15 m thick major channel sandstone complexes are present. Person for scale is *ca* 1·8 m tall. (G) Laterally continuous coal seams of the Tullock Member exposed in outcrops between Bug Creek and Purgatory Hill. (H) Somber, greenish weathered mudstones of the Hell Creek Formation overlain by coal-bearing light-brown siltstones of the Tullock Member with the lithostratigraphic boundary at the base of coal seam #1-Z in between Purgatory Hill and Rock Creek. The position of the KPB is probably at the arrowhead, in between the *in situ* preserved *Triceratops sp.* horn and #1-Z. Person for scale is *ca* 1.8 m tall. (I) Sets of decimetre-scale cross-bedded channel sandstones in the Tullock Member at Purgatory Hill North-east showing a palaeocurrent to the left. Black camera lens cover for scale (diameter = 5·7 cm).

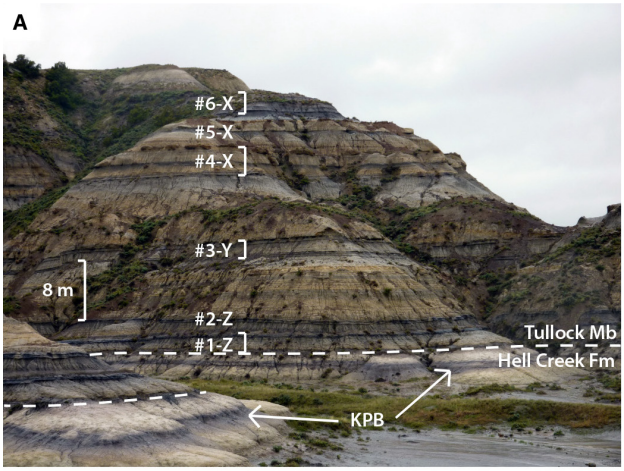

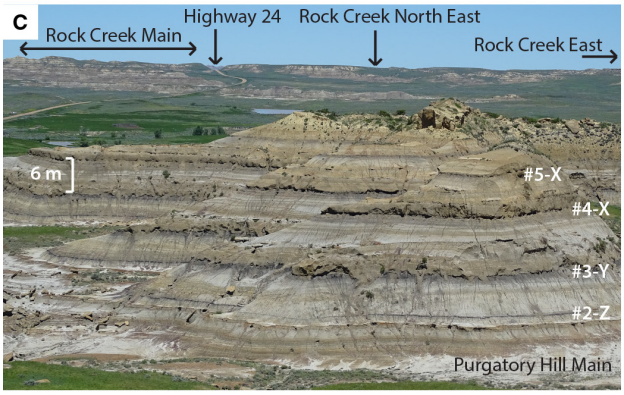

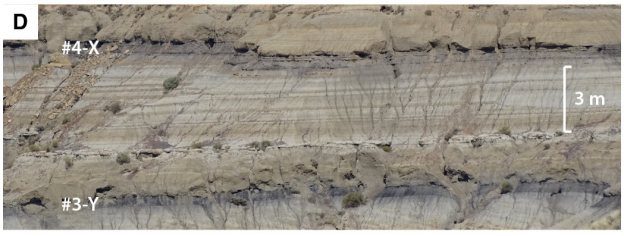

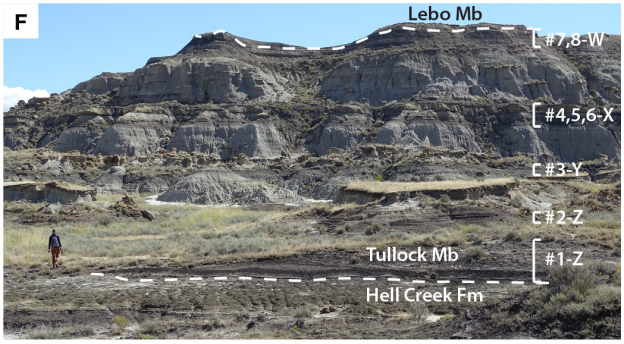

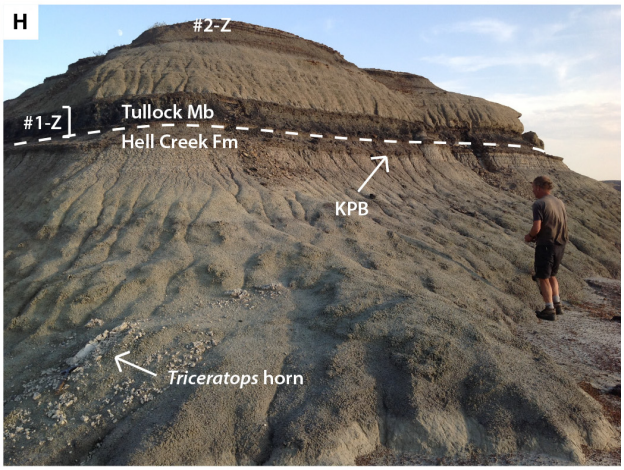

large sandstone bodies belonging to fluvial channels are not present in overbank composites as these were avoided. Distinct stratigraphic levels (such as volcanic ash layers, coal beds or siderite cemented horizons) were used to correlate individual trenches in the same outcrop. Next to the detailed overbank composite sections, single sections were logged to establish a lateral framework. These sections were logged at *ca* 0·75 km intervals between the areas of the composite sections; they were measured directly on the outcrop, from base to top, and thus reflect the local bottom to top succession including possible channel sandstones. All section abbreviations are defined in Fig. 1. The NNE–SSW-oriented transect of the framework is perpendicular to the ESE, but approximately parallel to the north average palaeocurrent directions of channel belts (Fig. 1), which were determined from decimetre thick sets of medium-grained cross-bedded sandstone in the central parts of channel fills.

The coal seams were correlated using distinctive tephra layers. The tephras are mainly composed of quartz, sanidine and plagioclase minerals but also moderate amounts of biotite, titanite and zircon can be present. The crystals typically have euhedral shapes, distinct from rounded detrital grains. Four characteristic tephras were commonly recognized in the sections along the transect based on their distinct colour, thickness, grain size and weathering. A grey sticky bentonite (GSB) with a thickness of *ca* 10 cm, altered to a massive claystone with typical popcorn-like weathering, occurs in the upper part of coal #1-Z. An orange rusty ash (ORA) with a thickness of *ca* 1 cm and a fine to medium grain size occurs in coal #3-Y. A pink straight ash (PSA) with a thickness of *ca* 1·5 cm and a fine grain size occurs in the uppermost part of coal #5-X. A white crumbly ash (WCA) with a thickness of *ca* 1 cm and a fine to medium grain size occurs in coal #8-W. Photographs of these tephras are shown in Fig. 3. Further details on the field methods are provided in Appendix S1.

Palaeomagnetism

A total of 207 levels were sampled for palaeomagnetic analysis within five composite sections. Oriented hand samples and standard palaeomagnetic cores of 2·54 cm diameter were taken with an electric, battery-powered drill using water as a coolant. Average sample spacing was between 45 cm and 66 cm with much higher resolution around the anticipated C29r/C29n magnetic polarity reversal (Swisher *et al.*, 1993).

Previous palaeomagnetic analysis of the Tullock Member in north-eastern Montana showed that secondary overprints were removed after demagnetization at 160 to 200°C or 10 to 30 m Tesla (mT) for thermal (TH) and alternating field (AF) demagnetization experiments, respectively

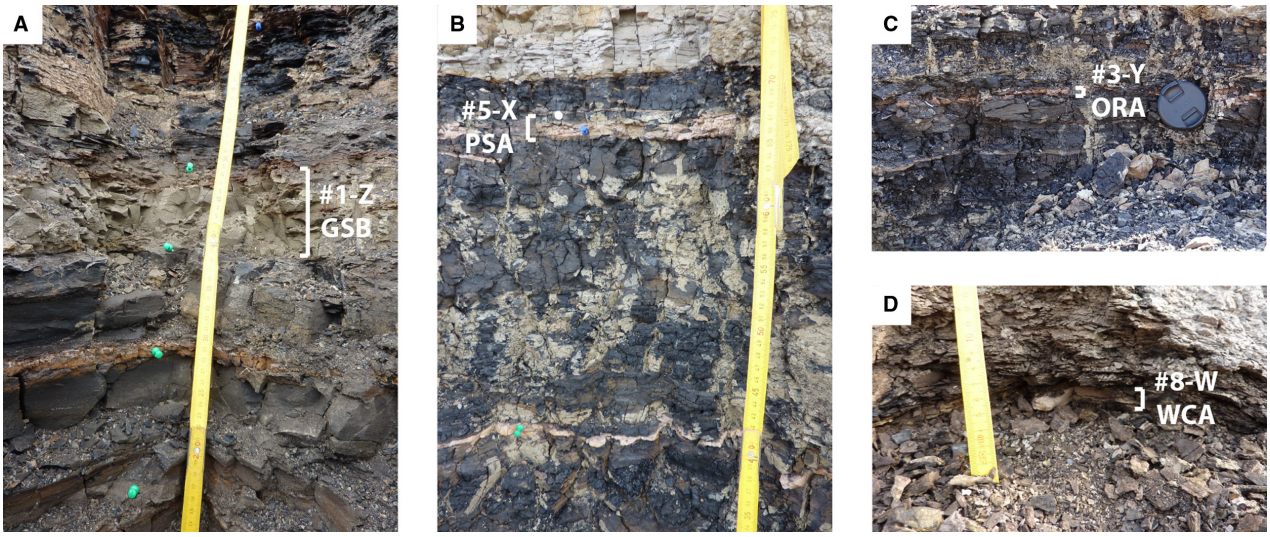

Fig. 3. Field photographs of four distinctive tephras used for coal correlation. (A) Grey sticky bentonite (GSB) in coal #1-Z. Pushpins (green) 10 cm apart. Bug Creek Main. (B) Pink straight ash (PSA) in coal #5-X. Pushpins (green and blue) 25 cm apart. Bug Creek Main. (C) Orange rusty ash (ORA) in coal #3-Y. Black camera lens is 5·7 cm in diameter. Rock Creek North-east. (D) White crumbly ash (WCA) in coal #8-W. Length of ruler on image is 17 cm. Bug Creek South-east. A description of these tephras is provided in the *Methods* section.

(Swisher *et al.*, 1993). Dominant magnetic remanence carriers included magnetite and maghemite (Sprain *et al.*, 2016) but also compositionally intermediate titanohematite can be present (Swisher *et al.*, 1993; Sprain *et al.*, 2016). The latter mineral is particularly known for its ability to show a self-reversal that could bias palaeomagnetic interpretations (e.g. Nagata *et al.*, 1951; Sprain *et al.*, 2016). Based on those earlier results, it was decided to use both TH and AF demagnetization. If sufficient sample material was available, sampling horizons were processed twice, once with TH and once with AF demagnetization. Otherwise, if only one sample was available and the core was not of sufficient length to split it into two parts, TH demagnetization was the method of choice. Samples were thermally demagnetized in a magnetically shielded furnace (residual field <10 nT) with steps of 20 to 30°C up to a maximum of 450°C. Alternating field demagnetization was applied in a magnetically shielded room with an in-house built robot with steps of 3 to 10 mT to a maximum of 100 mT (Mullender *et al.*, 2016). For both methods, the remanent magnetization was measured after each demagnetization step with a 2G Enterprises DC SQUID magnetometer (2G Enterprises, Sand City, CA, USA) with an instrumental noise level of *ca* $2*10^{-12}$ Am^2; typical NRM intensities were at least two orders of magnitude higher.

The palaeomagnetic data were analysed in Remasoft 3.2 (Chadima & Hrouda, 2006) and were plotted in an orthogonal projection, so-called Zijderveld diagrams (Zijderveld, 1967). The reversed polarity samples served as a template to establish maximum blocking temperatures and alternating fields for the secondary overprint and the characteristic remanent magnetization (ChRM) in the palaeomagnetic interpretation: directional differences between the overprint and ChRM are much smaller in normal polarity samples. The ranges of the secondary overprint removal are similar to Swisher *et al.* (1993). The ChRM was determined by anchored principal component analysis (PCA) (Kirschvink, 1980) for samples that showed a clear demagnetization trend towards the origin. A minimum of four consecutive points was selected in the PCA. The ChRM is considered reliable when the mean angular deviation (MAD) of the anchored fit is <15°. Samples with MAD > 15°, but with nonetheless a clear ChRM component, were retained in the magnetostratigraphic column since the mean of the data is weighted by the anchors of the PCA fit. These samples were considered of lower quality and displayed (Figure S2) with open circles, excluded from the connection line. Data that showed no clear trend towards the origin but mainly a clustering of higher coercivity vector end-points were analysed by taking a Fisher mean (Fisher, 1953).

Coal petrographic analysis

In total, 11 bulk samples and five *in situ* oriented pillars were prepared for coal petrographic analysis. Bulk samples analysed are one of #1-Z for Rock Creek Main (RCM), one of #3-Y for Rock Creek East (RCE), three of #3-Y for Purgatory Hill Main (PHM), four of #5-X and two of #6-X for Bug Creek South-east (BCSE). *In situ* pillars analysed are one of #1-Z for RCM, one of #3-Y for RCE, one of #1-Z for PHM, one of #5-X and one of #6-X for BCSE.

Crushed samples were prepared from bulk samples and embedded in polished blocks (35 mm diameter) according to industry standards; the full methodology is given in Robson *et al.* (2015). Small *in situ* pillars of varying sizes were prepared following the procedures of Collinson *et al.* (2007). The polished faces of crushed samples and *in situ* pillars were viewed in reflected light under oil immersion (Cargille type A, density 0·923 g cc^{-1} at 23°C, RI 1·514) using a Leica microscope (Leica, Wetzlar, Germany). A x20 oil immersion objective was used. Coal components (macerals) were identified according to International Committee for Coal and Organic Petrology (ICCP) standards (ICCP, 1963, 2001; Sýkorová *et al.*, 2005) and photographed with a 5 megapixel ProgRes Capture Pro 2.7 camera (Jenoptic, Jena, Germany). When analysing macerals in crushed samples, 504 points at 50 μm intervals along a transect were quantified. For *in situ* pillars, three transects were quantified with the same methodology as in Robson *et al.* (2015).

Vertical alignment of stratigraphic sections in the fence panel

Instead of using a fixed point (for example, KPB) to align all stratigraphic sections on the same level, an optimization approach was used to vertically compensate for differences in stratigraphic thickness throughout the fence panel. In this approach, three distinctive tephras were chosen as tie-points, i.e. the #1-Z grey sticky

bentonite (GSB), #3-Y orange rusty ash (ORA) and #5-X pink straight ash (PSA) that are all preserved in the Bug Creek Main (BCM) section. New stratigraphic positions of tie-points of the other sections were then calculated with respect to BCM. First, an offset to the tie-points was defined for each section and added to the original stratigraphic position of the tie-points. Subsequently, the absolute cumulative difference between tie-points of the reference and aligned sections was determined. In the Solver add-in function in MS Office Excel®, the absolute cumulative difference was set to minimal by changing the offset value to optimize mutual vertical positions.

Colour and grain size index (GSI) records

For each composite section, a colour reflectance record was produced at ≤5 cm resolution using a Minolta CM 600d portable photospectrometer (Konica Minolta, Tokyo, Japan). The automated average of three measurements per selected level was used. Measurements were always performed on freshly broken pieces of rock avoiding discoloration due to drying or oxidation.

A grain size index (GSI) was developed based on the lithology determined during logging (Fig. S1). Each lithological unit was assigned a single value on a linear scale between 0 and 4 to make the index. Nine values were used: 0 – coal; 0·5 – carbonaceous shale; 1 – clay; 1·5 – mud; 2 – silt; 2·5 – very fine sandstone; 3 – fine sandstone; 3·5 – medium sandstone; and 4 – coarse sandstone. For units with multiple grain sizes (for example, sandy siltstone), the dominant grain size value (in this case, 2 for silt) was used. The GSI records are presented alongside the simplified logs (Fig. 8).

Decompaction

A correction for compaction is needed in cyclostratigraphic analysis of coal-bearing successions, since post-depositional peat compaction is larger than compaction of clastics. A compaction ratio of 4 : 1 was obtained using silicified peat from a lignite layer in the Upper Fort Union Formation in North Dakota (Ting, 1972, 1977). The same compaction ratio of 4 : 1 was also suggested by Cherven & Jacob (1985) for coal seams of the Western Interior Zuni sequence. This should be considered a minimum compaction since compaction due to early-stage dehydration before depositional overburden will increase the ratio. Pre-lithostatic compaction is not taken into account because quantitative estimations of this parameter are lacking in literature.

Using standard compaction curves of Baldwin & Butler (1985), that are based on marine sediments (Sclater & Christie, 1980), lithostatic compaction for shales and sandstones in the Tullock Member has been determined at, respectively, 75% and 88% of the original thickness (Retallack, 1994). However, decompaction based on the compaction curves of Baldwin & Butler (1985) is not realistic for floodplain successions and decompaction can be even overestimated by as much as 34% (Nadon & Issler, 1997). Therefore, compaction of shales and sandstones was probably significantly less than was proposed by Retallack (1994). In this study, the compaction of shales and sandstones cannot be reliably estimated but is assumed to be negligible with respect to the lithostatic compaction of peat. The coals in the GSI overbank composite records were decompacted, with a decompaction factor of four, to account for the impact of peat compaction on stratigraphic thicknesses.

Cyclostratigraphic analysis

A commonly used method for analysing cyclicity in sedimentary successions is spectral analysis, breaking a stratigraphic signal into its individual frequency components. The outcome of spectral analysis is generally shown in a power spectrum, showing the power spectral density (or power) against decreasing frequency, or against increasing periodicity, i.e. $(\text{frequency})^{-1}$. The spectrum better represents different scales of cyclicity if the proxy record (i.e. signal) is of sufficient stratigraphic resolution and if the proxy record is able to trace the stratigraphic changes of interest. In this study, lightness (L*) and yellowness (b*) colour and grain size index (GSI) records, of three overbank composite sections, trace changes in lithology at centimetre-scale resolution. Spectral analysis has been applied to undecompacted L*, b* and resampled GSI records and decompacted, resampled GSI records using the REDFIT procedure (Schulz & Mudelsee, 2002). Further explanation of data re-sampling and settings used in REDFIT is provided in Appendix S1.

The power spectra of the overbank composite records were compared with a histogram of the fence panel (Fig. 7), where the histogram shows the thickness distributions of typical alternation scales of main lithofacies along the fence panel

transect (Fig. 6). In this way, the significance of local overbank cyclicity was tested with respect to regional thickness variations. Ranges of significant cyclicity were subsequently isolated from the records using Gaussian bandpass filtering in Analyseries 1.1.1 (Paillard *et al.*, 1996), and overlain on the original record to examine the origin of these cycles.

RESULTS

The palaeomagnetic results are presented first, because the polarity reversal is an important tie point for correlations of the three composite sections in McCone County. Then, the coal petrographic results are described and the environmental settings are inferred. Subsequent sections successively deal with the stratigraphic fence panel, time-stratigraphic correlation, lateral thickness variations and the scale of sedimentary successions. In the final section, the power spectra of the overbank composite proxy records are compared with the histogram of the fence panel. This is followed by an interpretation of the filtered periodicities and significance of cyclostratigraphic results after decompaction.

Palaeomagnetism

Figure 4 shows characteristic NRM demagnetization results. The starting NRM ranges from *ca* 500 to *ca* 1500 $\times 10^{-6}$ A m^{-1}. The majority of the samples are essentially demagnetized at *ca* 400°C or 100 mT with remaining NRM mostly <150 $\times 10^{-6}$ A m^{-1}. A stable primary ChRM component can be isolated in most reversed polarity samples upward from 180°C (TH) or 20 mT (AF) (Fig. 4): 61·3% of the total directions showed a clear ChRM component directed towards the origin and were calculated with an anchored-PCA fit. The remaining directions (38·7%) showed a clustering of higher coercivity vector end-points and were calculated with a Fisher mean. The polarities can be divided into four groups: (i) reversed polarity (30·5%); (ii) normal polarity (42·2%); (iii) uncertain polarity (13·5%); and (iv) undetermined polarity (13·8%). The difference between the present-day overprint and the ChRM in normal polarity samples is difficult to isolate. On the reasonable premise of similar unblocking behaviour of reversed and normal polarity samples, 180°C or 20 mT was also taken as ChRM threshold (Fig. 4). Samples with an uncertain polarity show inclination and declination angles in between normal and reversed samples and/or clustering of vector end-points around, or close to, the origin (Fig. 4). Undetermined polarity includes samples with no interpretable ChRM component. The TH and AF magnetostratigraphic data are provided in Appendices S2 and S3. Raw TH and AF palaeomagnetic data are available online in the data repository of this article.

In the palaeomagnetic polarity plots (Fig. S2 A to E), ChRM components of samples from the KPB until the top of coal #4-X show a clear reversed polarity with southward declination and negative, upward, inclination. The ChRM components of samples approximately 1 m below coal #5-X to the stratigraphically highest samples (*ca* 1 m below coal #8-W in BCSE) show a normal polarity with northward declination and positive, downward, inclination. The RCE, PHM and BCM sections consistently show an uncertain polarity interval above coal #4-X to just below (*ca* 1 m) coal #5-X (Fig. S2). These samples yield a relatively weak ChRM (*ca* 250 $\times 10^{-6}$ A m^{-1}) when compared to clearly reversed and normal samples (typically around *ca* 700 $\times 10^{-6}$ A m^{-1}). Based on the comparison with earlier magnetostratigraphic studies in the Western Interior Williston Basin (Swisher *et al.*, 1993; Peppe *et al.*, 2009; LeCain *et al.*, 2014) and the position of the KPB, the magnetic polarity pattern was correlated with the C29r/C29n polarity reversal.

Coal maceral assemblage

According to the ICCP classification standard, the three low-rank coal maceral groups are huminite, liptinite and inertinite. Huminite (i.e. vitrinite in higher rank coals) is a main component (up to 90%) in Cenozoic brown coals that forms when woody tissues of plants and trees are anaerobically preserved (Sýkorová *et al.*, 2005). Liptinite is derived from algal and bacterial material, as well as from plant organs with high hydrogen contents such as spores and cuticles (Teichmüller, 1989). Inertinite in low-rank (lignite) and medium-rank (bituminous) coals has higher reflectance than huminite or liptinite in reflected light (ICCP, 2001).

Inertinite maceral percentages and other maceral quantifications

Coal maceral groups recognized in both the crushed samples and *in situ* pillars are the huminite group (average 80%) followed by

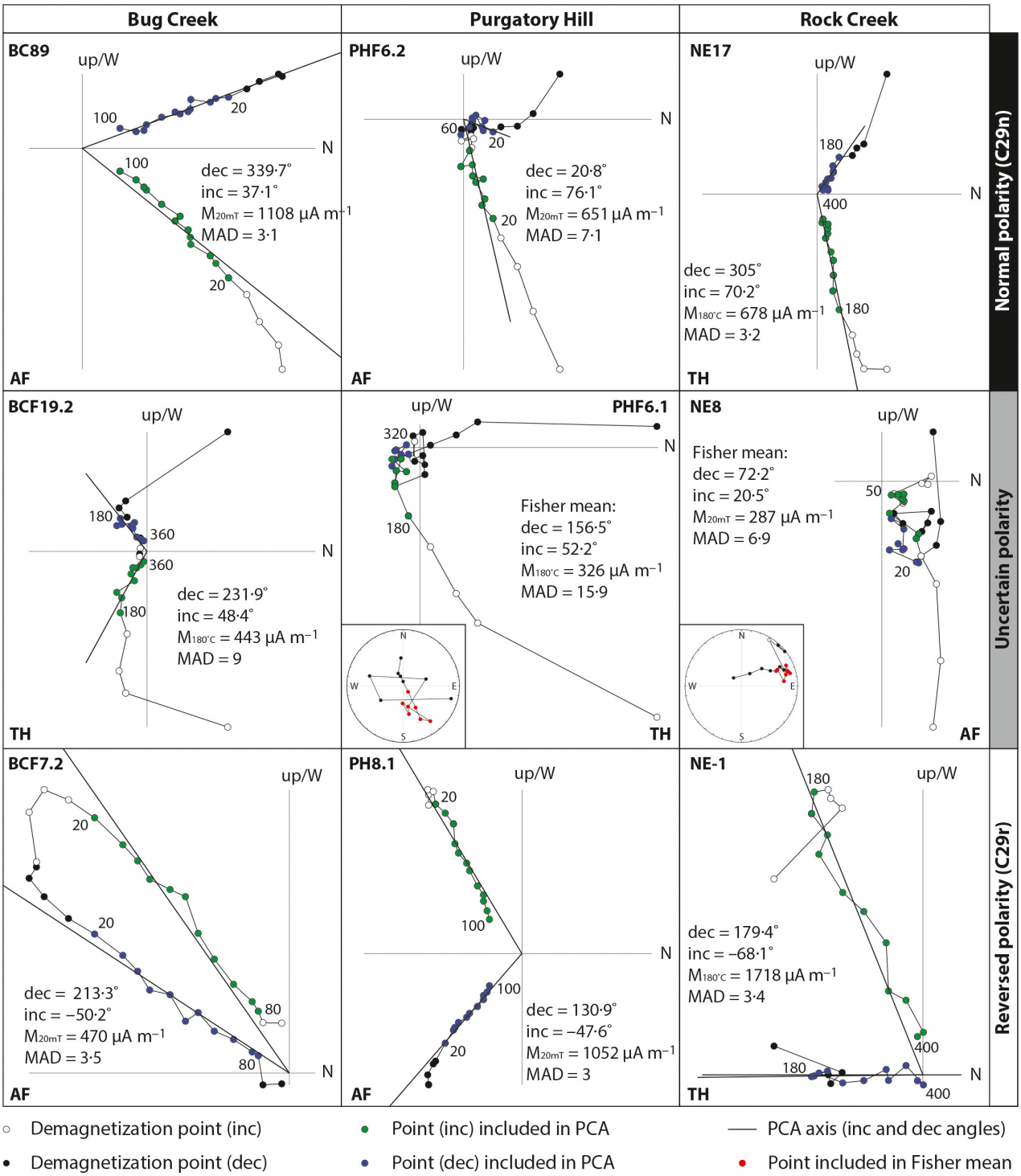

Fig. 4. Zijderveld diagrams of TH and AF demagnetized samples characteristic for the magnetostratigraphy of the Tullock Member at Rock Creek, Purgatory Hill and Bug Creek. In samples with a clear reversed polarity, stable ChRM components of inclination (inc) (open circles) and declination (dec) (solid circles) were isolated from the secondary present-day overprint component upward from 180°C (TH) and 20 mT (AF). Samples with a normal polarity were interpreted assuming similar unblocking spectra of the ChRM component. Points included in the anchored PCA are indicated for declination (blue) and inclination (green). In two panels (middle and middle-right), equal area plots have been included since these directions are calculated with a Fisher mean. Points included in the Fisher mean are indicated in red. Magnetostratigraphic polarity plots of inclination, declination and ChRM intensity for the different composite sections are shown in Figure S2 (A to E).

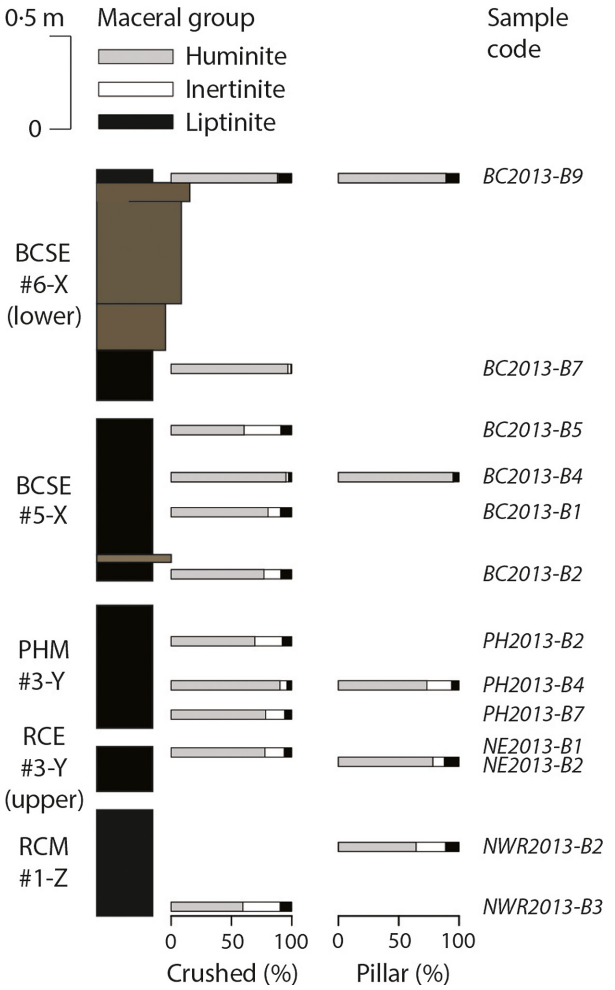

Fig. 5. Summary of quantified maceral group percentages per crushed, or *in situ* pillar coal sample (all maceral percentages are provided in Appendix S4). Coal seams in the Tullock Member are dominated by huminite (*ca* 80%). Inertinite (i.e. charcoal) is present in all samples (≤1% cannot be shown in scale of the diagram) indicating wildfire activity across the area and throughout the time interval studied. Variation in inertinite percentages between 1% and 31% suggests that wildfire activity varied throughout the succession.

inertinite (average 12%) and liptinite (average 8%) (Fig. 5). The most common inertinite macerals present are fusinite, semi-fusinite and inertodetrinite. In fusinite and semi-fusinite particles, only cell walls show higher reflectance than surrounding huminite. Fusinite and semi-fusinite particles often show bogen structures (brittle fracturing displacing cell walls). The highest percentages of inertinite occur in samples NWR2013-B2 and NWR2013-B3 of RCM coal #1-Z (31% in the crushed sample, 24% in the *in situ* pillar), in sample PH2013-B2 of PHM coal #3-Y (23% in the crushed sample) and in sample BC2013-B5 of BCSE coal #5-X (31% crushed sample). The most common huminite macerals are ulminite, attrinite and textinite. Quantitative data on all macerals are provided in Appendix S4 with example images of macerals in Fig. S3.

Environmental interpretation

Multiple evidence shows that inertinite macerals are products of wildfire activity, i.e. charcoal (e.g. Scott & Glasspool, 2007; Scott, 2010, and references cited therein). The average of 12% inertinite in coal seams of the Tullock Member is slightly lower than the 17% of inertinite in Palaeocene coals (Glasspool & Scott, 2010), but still significantly higher than inertinite percentages in coal seams of the early Eocene (Robson *et al.*, 2015). The inertinite percentages of the samples range from 1 to 31%, suggesting that wildfire activity significantly varied throughout the succession. The range of inertinite macerals (fusinite, semi-fusinite and inertodetrinite) present suggests derivation from local fires rather than distant regional fires (Glasspool & Scott, 2010). The general lack of high-reflecting cell infills and presence of bogen structures indicates that the inertinite was formed prior to decomposition of the plant material. The five small *in situ* pillars studied did not contain evidence of burned peat surfaces. Generally, abundant ulminite in the total maceral assemblage indicates predominantly wet conditions within forested peatlands (Diessel, 1992; Sýkorová *et al.*, 2005). Large wood particles, present in inertinite (Fig. S3 A and C) and in textinite (Fig. S3 D), indicate the presence of woody plants in the peatlands.

Stratigraphic fence panel

Logs of the composite and single sections in the NNE–SSW-oriented fence panel (Fig. 1) are plotted at a 1 : 60 000 horizontal scale and a 1 : 400 vertical scale (Fig. 6). Sections have been aligned vertically according to methods described earlier. Two lithostratigraphic boundaries are shown within the fence panel: the Hell Creek–Tullock and the Tullock–Lebo Shale boundaries. Within the Tullock Member, three units are shown. Each unit mainly represents one of the three main lithofacies of the Tullock Member (Table 1). The major coal seam intervals predominantly contain lithofacies C (mire

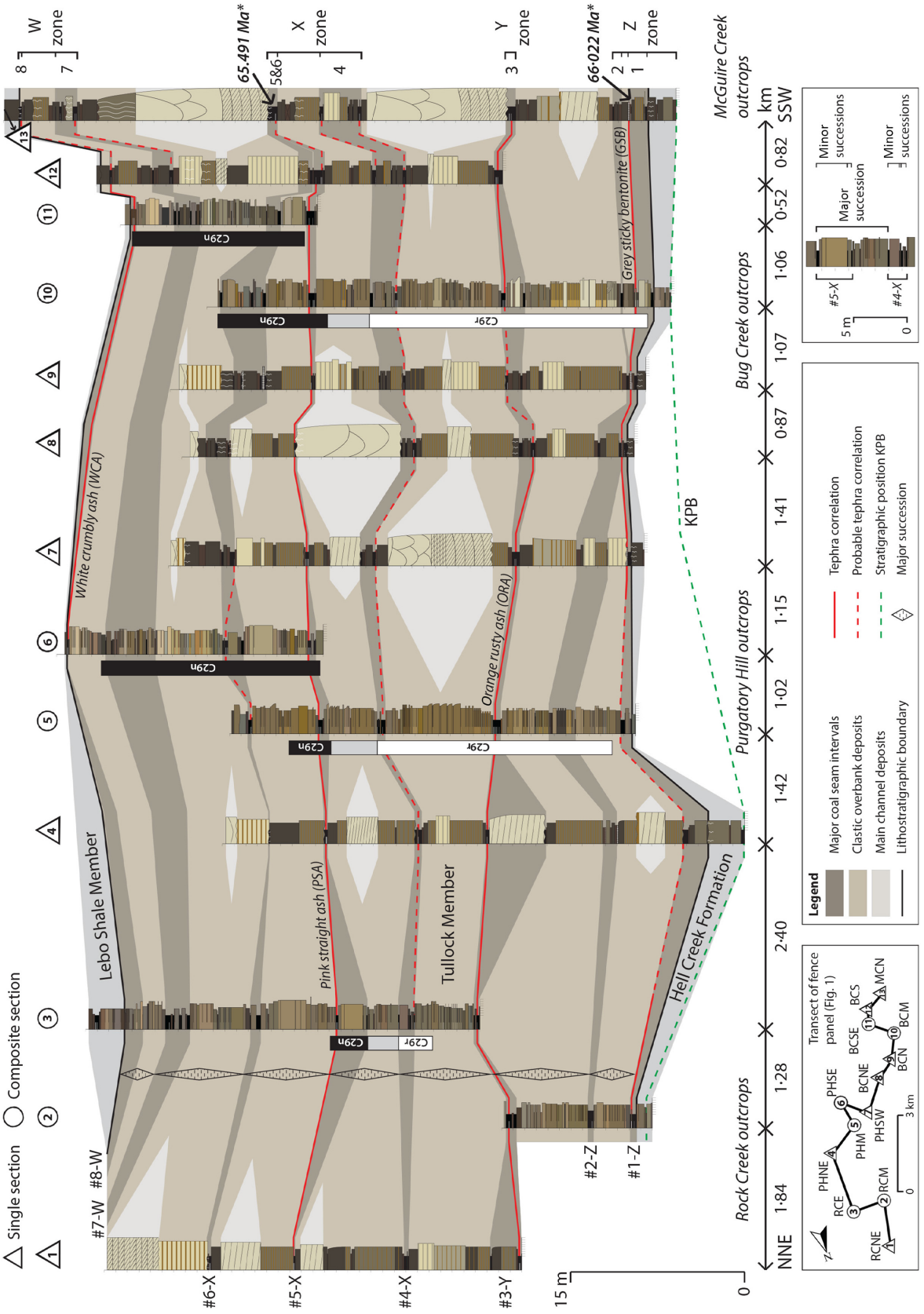

facies). The clastic overbank deposits predominantly contain lithofacies B (splay facies). The main channel deposits predominantly contain lithofacies A (channel facies). Detailed descriptions of sub-facies within the three main lithofacies are provided in Table 1.

Correlation of the distinctive tephras shows lateral continuity of the major coal seams between the sections. No major changes in the stratigraphic position of the ash layers within the coal seams were observed, with the exception that the Grey Sticky Bentonite (GSB) was not observed in the area of Purgatory Hill, in between the PHSW and RCM sections (Figs 1 and 6). Disappearance of GSB in the central area of Purgatory Hill may be attributed to erosion by the emplacement of crevasse splay complexes, an example of which is observed close to the PHSW section. Stratigraphic consistency of coal seams is supported by the position of the C29r/C29n reversal at RCM, PHM and BCM, between coal #4-X and coal #5-X (Figs 6 and S2). Lateral continuity of the numerically labelled coal seams (for example, #3-Y) up to 10 km is in agreement with the traceability of these coal seams in the field (for example, Fig. 2G). Interfingering channel sandstones do not interrupt lateral continuity of the major coal seams. The major clastic facies and major peat facies mainly alternate vertically. The scarce coal seams in the uppermost part of the Hell Creek Formation mostly lack lateral continuity. This interval probably comprises isolated coal lenses that occur at comparable stratigraphic positions. The position of the KPB in BCM was correlated lithologically to RCM, PHNE and MCN. At these sites, the approximate position of the KPB is placed in the uppermost Hell Creek Formation, at the base of a coaly layer, a few decimetres to a few metres below #1-Z.

Major and minor successions

Two scales of successions were defined in the stratigraphic fence panel (right-bottom panel in Fig. 6). Major successions are 6·8 m thick on average and consist of basal clastic overbank or channel deposits overlain by a coal seam interval corresponding to a numerically labelled major coal seam (for example, #3-Y). Stratigraphically, from the top of coal #1-Z to the top of coal #8-W, seven successive major successions are recognized in the fence panel (Fig. 6). The total number of major successions measured from the 13 sections is 58. Along the fence panel, major coal seams generally do not merge, with the exception of the merging of coal #2-Z with coal #1-Z between PHSW and BCM and merging of coal #6-X with #5-X between BCS and MCN (Fig. 6).

Splitting of major coal seams into two or more minor seams occurs locally, with lateral persistence of splitting ranging from a few metres up to several hundreds of metres. Coal splits (i.e. the intercalated clastics) plus the overlying coal bed are herein referred to as minor successions (Fig. 6). The total number of minor successions measured from the 13 sections is 85. Within the fence panel, the thickness of minor successions varies from several metres (for example, a 4·8 m thick minor succession in #3-Y at the PHNE section, Figs 2B and 6) to a few centimetres (for example, a 4 cm thick minor succession in #5-X at the BCSE section). The thickness distributions of all minor and major successions measured from the 13 sections along the fence panel are shown in a histogram (Fig. 7). The thickness variation of the 85 minor successions with a mean of $0{\cdot}8 \pm 0{\cdot}7$ m is significantly higher than that of the 58 major successions (mean $6{\cdot}8 \pm 3{\cdot}7$ m). The thickness range of major and minor successions particularly overlaps between 1·3 m and 2·5 m (Fig. 7). Based on the mean, median and skewness of the data (Fig. 7), and according to Kolgomorov–Smirnov and Shapiro–Wilk normality tests, the major successions (total measured, from the 13 sections) are normally distributed. The same null hypothesis of a normal distribution for the minor successions (total measured, from the 13 sections) is rejected by these normality tests,

Fig. 6. Stratigraphic fence panel of the Tullock Member along the NNE–SSW transect (Fig. 1). Vertical positions of sections are calibrated using the optimization approach described in the text. Sections are correlated using the C29r/C29n polarity reversal between coals #4-X and #5-X and distinctive tephras such as the GSB in coal #1-Z, the ORA in coal #3-Y, the PSA in coal #5-X and the WCA in coal #8-W. The panel shows that major coal seams of the Tullock Member can be correlated over a distance of at least 10 km. Thickness variations are mainly caused by local and internal processes such as palaeorelief and differential peat compaction. Horizontal distances between the sections are indicated below the panel. * $^{40}Ar/^{39}Ar$ radioisotope ages are after Sprain *et al.* (2015).

Table 1. Lithofacies of the Tullock Member in north-eastern Montana.

Facies	Interpretation	Lithology	Internal structures	Colour and weathering	Unit boundaries
A – Channel					
A1	Major channel with high clastic loads and active infilling	Medium-grained (central fill) and fine-grained (marginal fill) sandstone in lower part of 5 to 10 m thick, isolated sandstone bodies	Vertically stacked sets of 40 to 100 cm thick trough cross-bedded layers with erosional bases (central fills) and 1 to 5 cm thick rippled cross-bedded layers (marginal fills)	Light-grey (2.5Y 8/1) sandstone, locally indurated and light-brown weathered. Erosional resistant cover sandstone	Sharp erosional base on top of underlying unit, generally not cutting through underlying lignite rank coal seams. Moderately gradual transition with overlying finer-grained deposits
A2	Minor channel with low clastic loads and active infilling	Fine to very fine-grained, muddy sandstone in upper part of 5 to 10 m thick, isolated sandstone bodies	Diagonally stacked decimetre to metre-scale multi-storey channel fills	Light-grey (2.5Y 8/2) sandstone, locally indurated and light brown weathered	Gradual transition with underlying coarser and overlying finer-grained units
A3	Small channels with episodically high clastic loads and active to abandoned infilling	Fine to very fine-grained muddy sandstone in 1 to 6 m thick isolated sandstone bodies	Decimetre to metre-scale multi-storey to single storey fills with lateral accretion planes and wedge-shaped fills	Light-grey (2·5Y 7/2) sandstone, locally indurated and light brown weathered	Sharp erosional base on top of underlying deposits. Gradual lateral transition with finer-grained deposits
B – Splay					
B1	Proximal splays	Decimetre-scale sequences of fine to very fine-grained sandstone beds fining upward to thin muddy sandstone beds in generally <6 m thick packages	Decimetre to centimetre-scale trough cross-bedding, erosional bases, small rootlets in silty layers	Light-grey (7.5Y 8/3) sandstone, locally indurated and light brown weathered. Greyish olive (7.5Y 6/2) muddy sandstone, light grey weathered	Sharp erosional base on top of underlying deposits. Gradual transition with overlying finer-grained deposits
B2	Distal, shallow lacustrine splays	Centimetre-scale sequence of sandy silt beds fining upward to mudstone beds in generally <6 m thick packages	Centimetre to millimetre-scale ripples and muddy laminae. Decimetre-scale interbedding of centimetre to millimetre thick cemented horizons (variegated). Rootlets present	Greyish olive (5Y 4/2) sandy silt and greyish olive (2.5Y 3/1) mudstone with interbedding of yellowish brown (10YR 4/7) cemented horizons (variegated)	Generally gradual transition with overlying coarser and finer-grained deposits
B3	Lacustrine splays	Siltstone to claystone in <2 m thick isolated elongated lenses	Homogeneous, finely (millimetre-scale) laminated silt and massive clay, some rootlets and slickensides at top of unit	Dark greyish olive (2.5Y 2/1), grey weathering	Gradual transition with underlying coarser-grained deposits but sharply overlying lignite rank coal seams

Table 1. (continued)

Facies	Interpretation	Lithology	Internal structures	Colour and weathering	Unit boundaries
C – Mire					
C1	Inundated forested mire with little clastic influx	Silty to muddy carbonaceous shale in <20 cm thick units	Heavily rooted and many slickensides	Dark-greyish-brown (5YR 2/2), platy weathering	Underlying or overlying lignite rank coal seams or as partings within lignite rank coal seams
C2	Forested mire with negligible clastic influx	Lignite rank coal in <1 m thick seams	*Ca* 10% to 50% bright (vitrain) bands with a conchoidal fracture (<2 cm thick). <2 cm thick tephra layers with euhedral crystals	Brownish black (10YR 1.7/1) to black	Sharply bounded with all other units. Roots penetrating into underlying unit(s)

and the histogram shows a positive skewed distribution.

Overbank cycles and significance in the fence panel

Overbank successions and determination of filters

The thickness range of major successions is less extreme for the individual overbank composite sections ROC and POC. For BOC, however, the thickness of 1·2 m for the major succession from top #1-Z to top #2-Z falls within the thickness range of minor successions. Significant spectral peaks, above 90% confidence level of the red noise estimate, occur within $\mu \pm 1\sigma$ of the Gaussian normal distribution, particularly in ROC and POC, and at $\mu \pm 1\sigma$, not overlapping with μ, particularly in BOC. The ranges of these peaks were chosen as bandwidths for the bandpass filters.

All filters representing the peaks within $\mu \pm 1\sigma$ of the Gaussian normal distribution essentially trace the major successions (Fig. 8). Such patterns are most clearly seen in the GSI and L* filtered records showing a one to one coal-filter fit for seven successive cycles in ROC (Fig. 8A) and POC (Fig. 8B). An exception is coal #7-W of POC which comprises two filtered cycles rather than one. Bandpass filtering indicates that the spectral peaks at $\mu \pm 1\sigma$ in BOC, and partly in ROC, are not compatible with the principal scale of the major successions.

Interpretations on the origin of the filters

The narrow, higher-frequency peaks at $\mu - 1\sigma$ (*ca* 3·2 m) probably originate from an overlap in thickness frequency between the minor and major successions (Fig. 7). This is suggested by the *ca* 3·2 m filters, tracing major and minor successions alternately along the records (Fig. 8). The 2·9 to 3·6 m filters for BOC are such examples showing half a cycle for the major succession from top-#1-Z to top-#2-Z and half a cycle for the minor succession in the #3-Y-coal split (Fig. 8C). The broad, lower-frequency peaks at 10·5 m ($\mu + 1\sigma$) in BOC, and partly in ROC, may also be related to the spectral power at *ca* 3·2 m because enhanced splitting into minor successions is likely to be followed by lower sedimentation rates, and vice-versa, due to compensational stacking as a function of local accommodation space. Compensational stacking was probably amplified by peat compaction and may be expressed by the high occurrence of major successions at $\mu \pm 1\sigma$ in the histogram, as well as the spectral peaks at $\mu \pm 1\sigma$

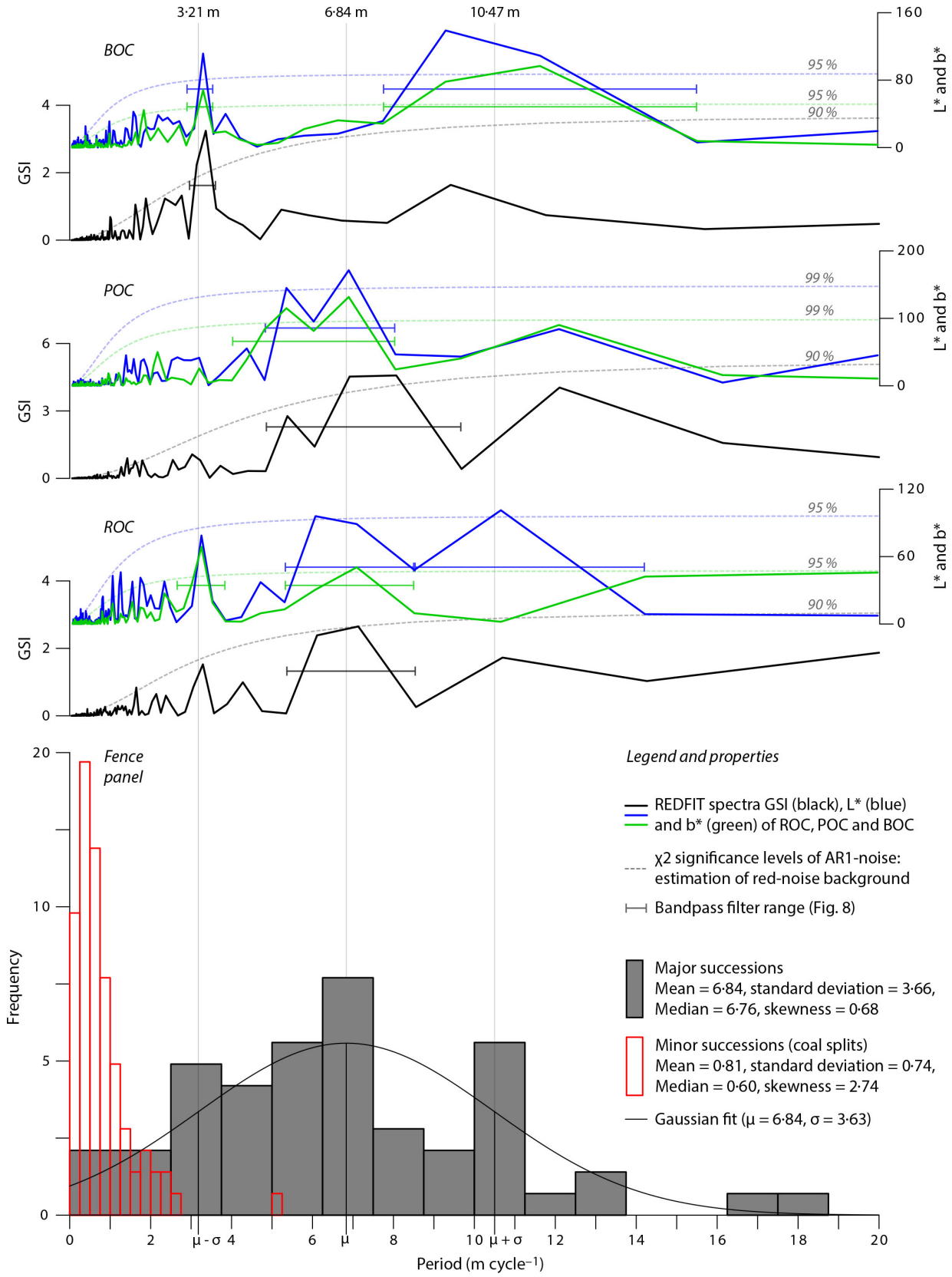

in BOC, and partly in ROC (Fig. 7). While the average 6·8 m thickness of major-scale sedimentation is the most significant cycle at Rock Creek and Purgatory Hill, the overbank sedimentation at Bug Creek was less regular at this scale.

Significance of spectral peaks after decompaction of coal

Spectral analysis of the 4 : 1 coal decompacted GSI records of ROC and POC shows higher significance of peaks (>95%) around the average of *ca* 8 m thick decompacted major successions (Fig. 9) when compared to the significance of peaks (>90%) in the undecompacted GSI records (Fig. 7). Spectral power at *ca* 8 m is also present in the decompacted GSI record of BOC but much less significant than at *ca* 3·5 m (Fig. S4). The filters of the decompacted GSI records show a more regular pattern (Figs 9 and S4) than the filters of the undecompacted records (Fig. 8). These results show that decompaction of coal results in higher significant power spectra and higher representative filters and thus implies more reliable cyclostratigraphic results when a decompaction can be reliably estimated.

DISCUSSION

It will be considered whether the results support the hypothesis of orbital-scale climate control on peat formation in the fluvial system interacting with autogenic processes. First, the stratigraphic architecture of the Tullock Member is addressed including the implications of the observed stacking pattern, its lateral continuity and forcing, and discrimination between the relative roles of autogenic and allogenic processes that might have produced the observed stacking patterns. Next, independent age control will be evaluated with respect to the significant major scale of cyclicity, to assess whether an orbital forcing model can be validated. Subsequent focus is on developing, presenting and evaluating conceptual models for orbital-scale climate control on peat formation in the fluvial system.

Stratigraphic architecture

Stacking and architectural elements

Except for local erosion by channels and splays, no major incisions with strongly developed palaeosols on the interfluves were observed within the fence panel of the Tullock Member (Fig. 6). This suggests the absence of: (i) major increases in fluvial gradient (channel incision); and (ii) prolonged non-deposition (palaeosol development) – two features that may be related to base-level lowering. Therefore, the Tullock Member differs from coal-bearing successions containing architectural elements that probably resulted from a lowering base level, such as the Pennsylvanian cyclothems in the Appalachian Basin of North America (e.g. Heckel, 2008; Cecil *et al.*, 2014), with sediment bypassing (unconformable surfaces) during the lowstands (Aitken & Flint, 1995), or the late Permian coal measures in the Bowen Basin of Australia, with clastic omission surfaces during the lowstands (Michaelsen & Henderson, 2000).

The Upper Carboniferous coal measures in the Campine Basin of Belgium show some resemblance to the Tullock Member. Vertical stacking in that Carboniferous succession also seemed to lack major non-depositional elements, although transitions between freshwater and marine environments were linked to relative sea-level changes (Paproth *et al.*, 1996), while such

Fig. 7. Lower part*:* Histogram of major (n = 58, grey) and minor successions (n = 85, red) from the 13 measured sections in the stratigraphic fence panel of the Tullock Member (Fig. 6). Bin widths of histograms were set to 0·25 m for minor and 1·25 m for major successions. The histogram of the major successions is normally distributed according to Kolgomorov–Smirnov and Shapiro–Wilk normality tests. Other parameters of the histograms (for example, mean, median and skewness) are also stated. Upper part*:* REDFIT spectra of ROC, POC and BOC for grain-size index (GSI), lightness (L*) and yellowness (b*). In the REDFIT spectra, significance of red noise background is estimated from a chi squared (χ^2) distribution of a first-order auto regressive function (AR1). Around the 6·84 m average of major successions in the fence panel, spectral peaks ≥90% of the red noise estimate occur entirely within $\mu \pm 1\sigma$ of the Gaussian normal distribution (particularly ROC and POC) and at $\mu \pm 1\sigma$, not overlapping with μ (particularly BOC). The spectral peaks in ROC and POC overlapping with μ could therefore be considered major successions significant in the stratigraphic architecture, which is in contrast to the peaks in the BOC record that do not overlap with μ. These peaks probably originate from an overlap in frequency between the minor and major successions. Both types of peaks are bandpass-filtered (ranges indicated on the figure) to reveal their origin; filter results are in Fig. 8.

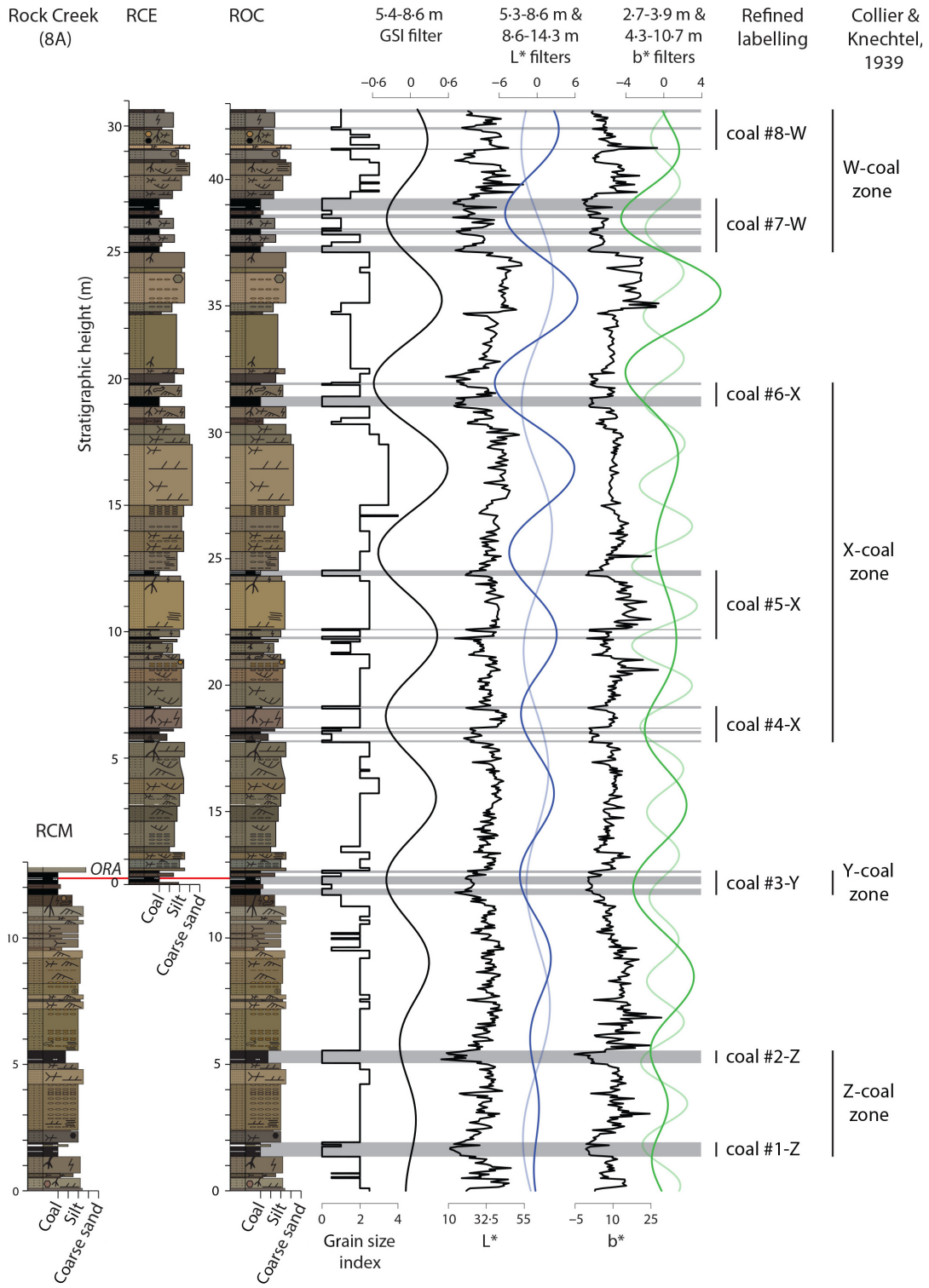

Fig. 8. Simplified composite logs of fluvial overbank successions in the Tullock Member exposed at Rock Creek (A), Purgatory Hill (B) and Bug Creek (C). In addition grain size index (GSI), lightness (L*) and yellowness (b*) records are shown. The Gaussian bandpass filters (ranges determined in Fig. 7) are shown to the right of each record. Filters for ROC and POC representing the peaks within $\mu \pm 1\sigma$ of the Gaussian normal distribution of the histogram (Fig. 7) essentially trace the major successions. Labelling of coal seams is in accordance with the refined coal nomenclature used in this paper and is shown with respect to the original coal scheme of Collier & Knechtel (1939). A legend to log symbols and characteristic Munsell colours is provided in Fig. S1 where the detailed sedimentary logs of the composite sections are given.

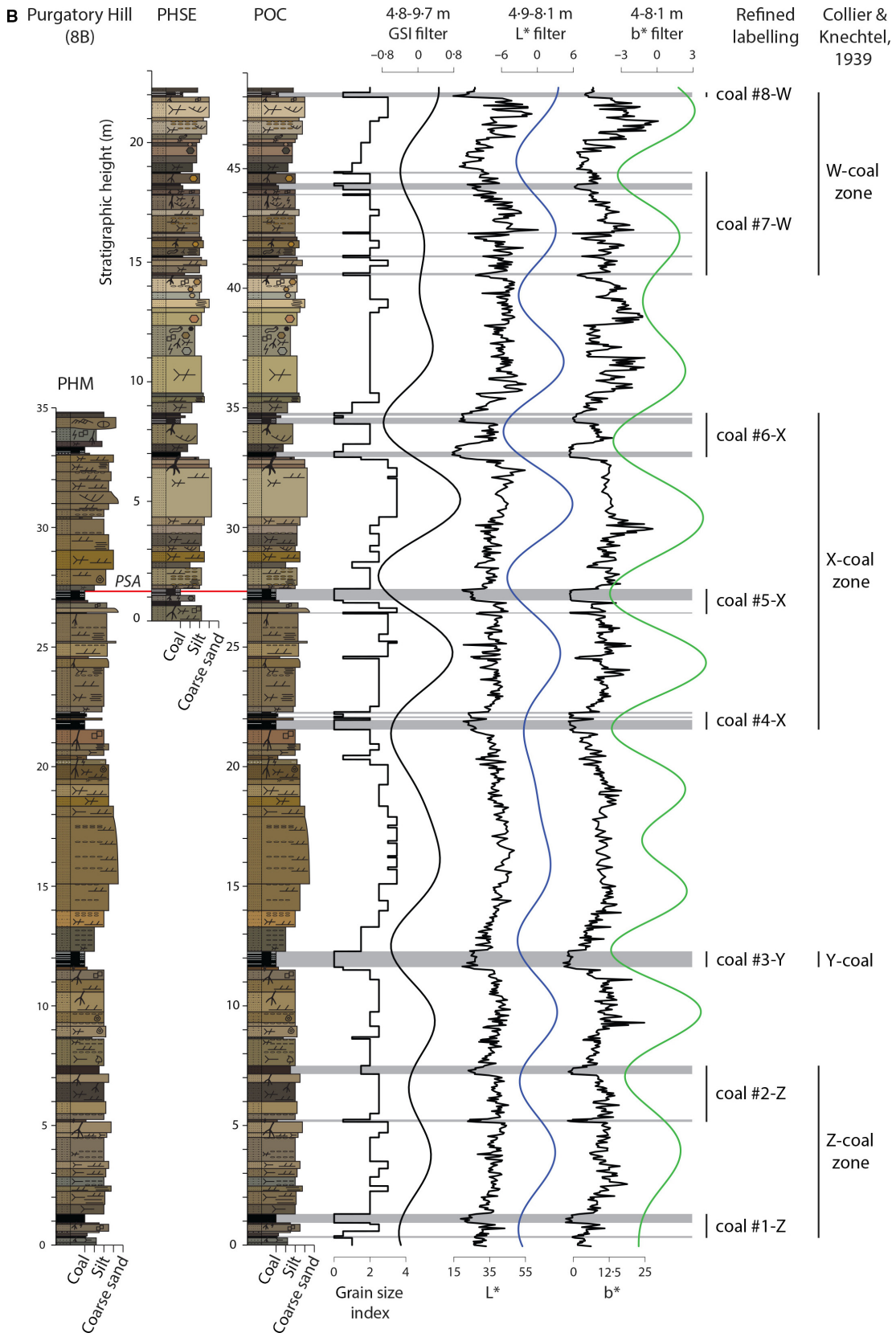

Fig. 8. Continued.

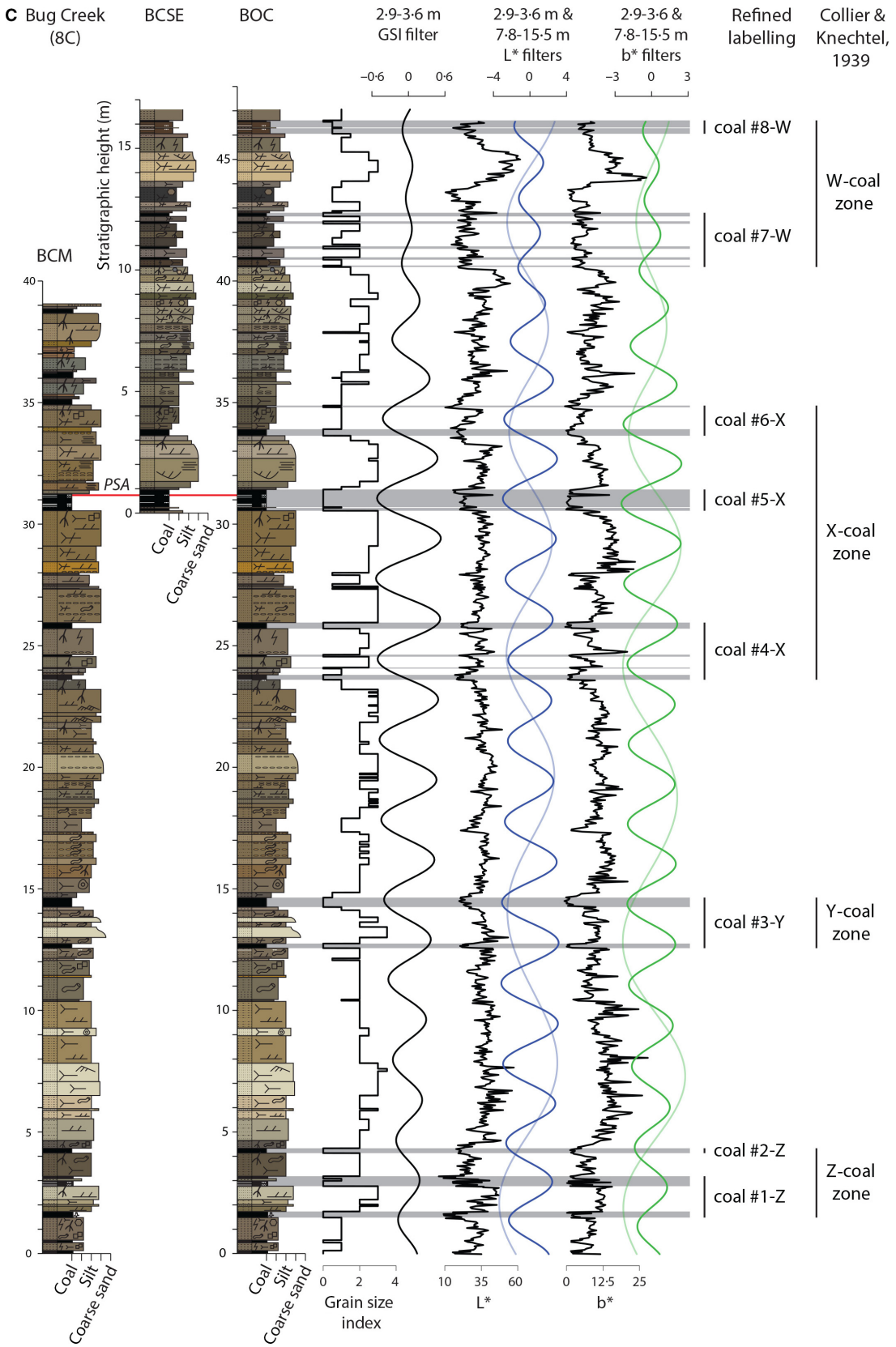

Fig. 8. Continued.

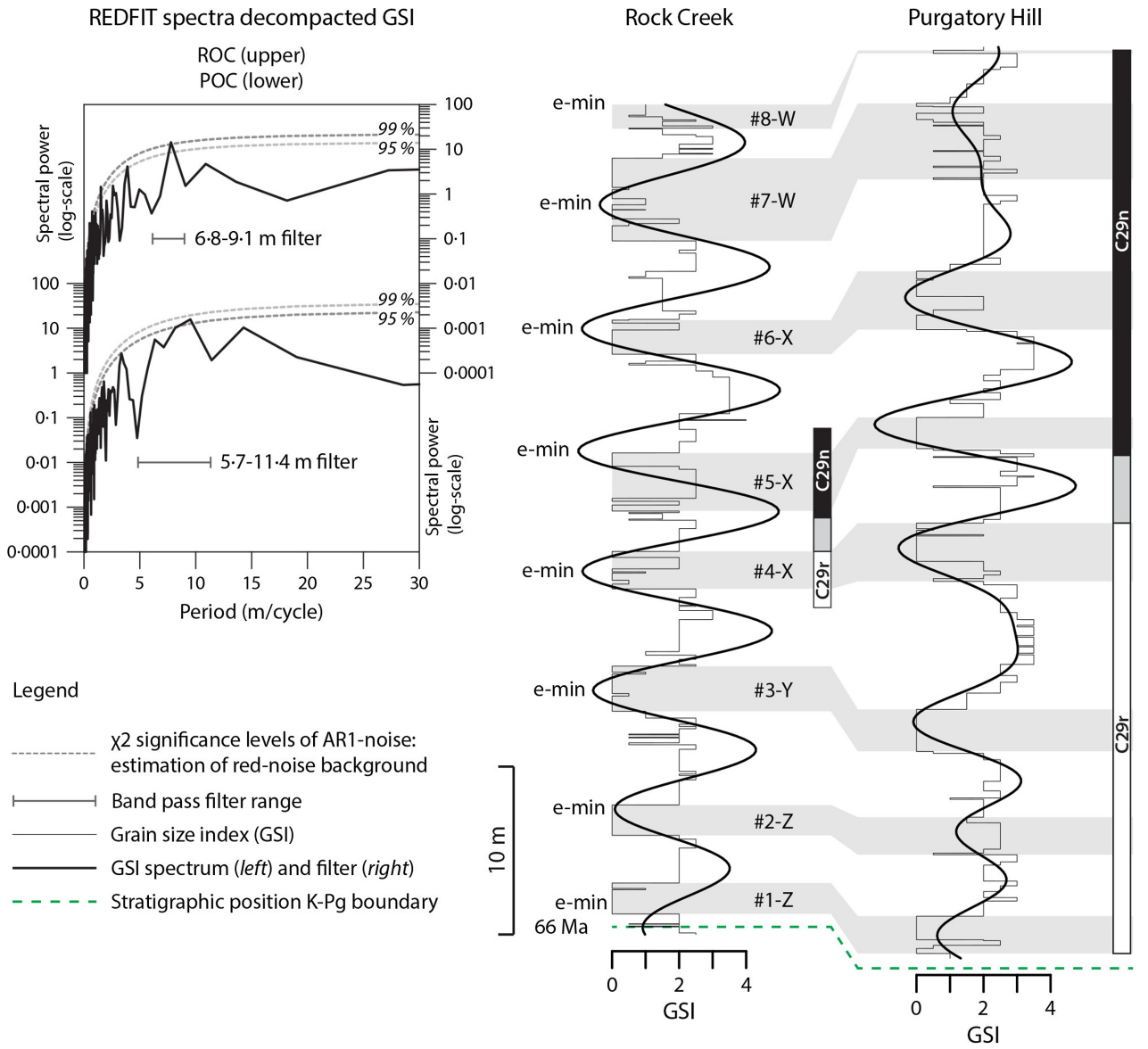

Fig. 9. Upper left part: REDFIT spectral analysis of the coal decompacted GSI records of ROC and POC (BOC is in Figure S4 because its significant frequencies were not compatible with the $\mu \pm 1\sigma$ of major successions; Fig. 7). Peaks show higher significance after the decompaction. Indicated filter ranges of significant spectral peaks at *ca* 8 m for both ROC and POC probably encompass the major peat-clastic overbank cycles. Right part*:* Corresponding Gaussian bandpass filters. The filters, tracing the coal decompacted major successions, may mimic 100 kyr eccentricity cycles with major peat formation during the eccentricity minima (e-min). Note that filter cycles do not always perfectly align and do not always show a 1 : 1 correspondence with major coal seams. This may be owing to local variations in sedimentation rate.

environmental shifts seem to be absent in the Tullock Member. Model simulations show that vertical stacking in coastal-plain environments can be the result of a balance between the rate of sea-level change and the rate of sediment supply (Cross, 1988). The vertical stacking in the Tullock Member could be the result of the same process. Subsequent to the KPB, increased rainfall leading to enhanced sediment supply (Fastovsky, 1987) and sea-level rise of the Cannonball Sea(s) (Sloan & Rigby, 1986) might have caused progradational and retrogradational shifts in equilibrium. This could have resulted in a relatively fixed coastline. The two main drainage directions of channel systems in the study area are to the north and to the east/south-east

(Fig. 1) and may point to a northern and south-eastern depocentre. This would imply that the Late Maastrichtian 'Dakota Isthmus' (Erickson, 1999; Hartman *et al.*, 2014) still existed in the earliest Palaeocene, separating the 'northern' and 'southern' Cannonball Seas.

Controls on thickness variations of major and minor successions

Locally, enhanced thickness variations of major successions might result from palaeorelief, such as that expressed by coal seam thinning and merging of major coal seams over main sandstone bodies, as observed in the south-western part of the fence panel (Fig. 6). The coal seam thinning may be related to palaeo-topographic highs where peat accumulation was less prolonged, whereas the alluvial ridge formed a barrier for siliciclastic sediment input (e.g. Davies-Vollum & Smith, 2008). Local depressions may have resulted from lithostatic compaction of thick peats during initial clastic sediment overburden. These areas may have facilitated channel development since sediments supplied during flooding events could have been transported to topographic lows. Channel developments at local depressions in the peat-forming area may be expressed by the channel complexes above coal #3-Y and above coal #4-X, in between PHM and BCM in the fence panel (Fig. 6). At the smaller scale, the discontinuous nature of coal splits (for example, Fig. 2B), along with the variable thickness range of minor successions (0·8 ± 0·7 m), suggests a stronger control by autogenic processes (for example, avulsion). These alternations cannot be adequately constrained from the current horizontal-scale resolution of the fence panel (Fig. 6).

Age control and orbital forcing

The transition from reversed to normal polarity, between coals #X-4 and #X-5, is correlated with the C29r/C29n reversal with a combined $^{40}Ar/^{39}Ar$ radioisotope and astronomical age of 65·69 Ma (Vandenberghe *et al.*, 2012) and a $^{206}Pb/^{238}U$ radioisotope age of 65·747 ± 0·043 (2σ) Ma or 65·801 ± 0·038 (2σ) Ma (Clyde *et al.*, 2016). The $^{206}Pb/^{238}U$ radioisotope ages of Clyde *et al.* (2016) were measured from a volcanic ash layer preserved within the C29r/C29n reversal interval of a core (*ca* 65·801 Ma) and an outcrop (*ca* 65·747 Ma) in the Denver Basin (Colorado, USA). The correlation of C29r/C29n is confirmed by the $^{40}Ar/^{39}Ar$ radioisotope ages of two tephras that were dated at McGuire Creek (*ca* 2 km south of Bug Creek) by Sprain *et al.* (2015). These tephras were also recognized in most sections of the present study area based on stratigraphic position and lithological characteristics. The older tephra, with an age of 66·022 ± 0·038 (1σ) Ma, occurs just above the base of #1-Z, generally a few centimetres below the grey sticky bentonite (GSB) (Fig. 6). The younger tephra, with an age of 65·491 ± 0·032 (1σ) Ma, occurs in the upper part of the X-coal zone, in an interval of multiple closely spaced ash layers. Since coal #5-X and coal #6-X merge in this area, this ash might correlate with the pink straight ash (PSA) in #5-X but could also belong to #6-X (Fig. 6).

According to $^{40}Ar/^{39}Ar$ ages of Sprain *et al.* (2015), the duration of the interval between the #1-Z-coal (*ca* 66·022 Ma) and the upper X-coal zone (*ca* 65·491 Ma) is 531 kyr. This duration accounts for approximately five to five and a half short-eccentricity cycles and covers either four (if from #1-Z to #5-X) or five major successions (if from #1-Z to #6-X) in the fence panel (Fig. 6). The duration of 531 kyr over five major successions is consistent with major coals seams of the Tullock Member being controlled by short 100 kyr eccentricity climate forcing. If all major coal seams follow 100 kyr cycles, and starting with an age of 66·022 Ma for coal #1-Z (Sprain *et al.*, 2015), the age of the C29r/C29n reversal in between coal #4-X and coal #5-X is calculated to be between *ca* 65·7 Ma and *ca* 65·6 Ma. This is consistent with 65·69 Ma (Vandenberghe *et al.*, 2012) but younger than 65·747 Ma or 65·801 Ma (Clyde *et al.*, 2016). Increased age control is needed to further assess the durations of the seven major successions.

Impacts of orbitally forced climate changes on fluvial systems evaluated in the context of the Tullock Member

Orbital-scale climate control on fluvial systems could be evident in systems that are sensitive to climate and, especially, to climatic control on sedimentary thresholds. Clastic sedimentation may be regionally intensified when seasonal precipitation increases, causing peak discharges that frequently exceed the threshold for crevasse splaying and channel avulsion. The 100 kyr short-eccentricity cycle may control such a threshold via the amplitude modulation of precession. The influence of the short-eccentricity-scale climate control on peat formation in fluvial

systems could therefore be evident because the threshold for mire degradation and regional-scale clastic sediment influx may be only exceeded at times of highest amplitude precession minima during high eccentricity. Orbitally forced climate changes may impact fluvial systems by pacing and intensifying autogenic processes at a regional scale and also by enhancing episodic sedimentation patterns as the result of increased contrasts in sediment supply. Previous research investigating these relationships is discussed and evaluated in context of the Tullock Member.

Orbital-scale climate control on the timing and intensification of autogenic avulsions

Based on integrated stratigraphic constraints and system analysis, Abels *et al.* (2013) proposed that autogenic avulsion patterns in the fluvial sequence of the Lower Eocene Willwood Formation in the Bighorn Basin (Wyoming, USA) were paced by precession-scale climate change. Abels *et al.* (2013) hypothesized two phases. During one phase, with relatively stable channel belt positions, channel belts were aggrading faster than the surrounding clastic floodplains. During the other phase, regional-scale avulsions were triggered by superelevation of the channel belt. Net sedimentation rate in the basin was hypothesized to have come sufficiently in pace with the basin subsidence rate to allow precession-scale climate change to drive these 'overbank-avulsion' cycles (Abels *et al.*, 2013).

A similar scenario, of net sediment deposition in the basin resulting from orbitally controlled climate change more or less in equilibrium with the subsidence rate, may also account for the sedimentary changes observed within the Tullock Member. However, in the Tullock Member, in contrast to the avulsion process in fluvial systems mainly composed of clastic material, compaction of underlying peat layers in response to channel infill initially offers additional accommodation that might delay avulsion. Van Asselen *et al.* (2009) postulated multiple influences of peat compaction on river behaviour. When, after some time, the compaction rate as well as the accommodation space of the channel decrease, the channel may migrate laterally (mechanism 1 in Van Asselen *et al.*, 2009). If the peats have high cohesive power, they may resist lateral migration of the channel belt leading to aggradation and, if accommodation in the channel becomes low, increased crevasse splaying (mechanism 2 in Van Asselen *et al.*, 2009). The coal seams of the Tullock Member probably originated from low-lying mires (Fastovsky, 1987) and, under the premise of small yearly changes in rainfall, peat formation would be expected to keep pace with channel belt aggradation. Floodplains would then only become more sensitive to crevasse splaying if the peat oxidized (and consolidated) above a lowering groundwater table (mechanism 3 in Van Asselen *et al.*, 2009). During dry periods, wildfires can burn across mires and down into the peat, creating topographic low areas that can become flooded if nearby a levée or channel, resulting in a so-called 'fire splay' (Staub & Cohen, 1979). The weight of such a splay deposit, on top of a dehydrated peat layer could cause differential compaction triggering the channel to avulse into the depression. Channels will be diagonally stacked in accordance with the classic autogenic model of avulsion controlled by peat compaction (Fielding, 1984). In the Tullock Member, peat compaction leading to splaying and avulsion could have been regionally triggered if peat consolidation during dry periods (which might have included wildfires) resulted from a response to orbitally forced climate changes. A regional-scale (possibly climatic) control on wildfires has been suggested, based on inertinite distribution patterns in coal seams across the KPB in the Ravenscrag Formation in Alberta and Saskatchewan (Jerrett *et al.*, 2015). The inertinite macerals in coal samples of the Tullock Member (Fig. 5; Appendix S4; Fig. S3) are likely to have been formed by the burning of non-decomposed vegetation. Because there is no evidence that the peat surface burned, the fires may only have affected the vegetation above the peat surface. Although fires might have been associated with drying and consolidation of peat, there is no direct evidence that this was the case during the deposition of the Tullock Member.

Orbital control on sediment supply and episodic sedimentation

The interfingering major channel sandstone bodies that do not interrupt the lateral continuity of major coal seams, combined with major coal seams and major channel sandstones succeeding one another in the fence panel (Fig. 6), might also depict a sedimentary system that was primarily controlled by upstream changes in sediment supply. Phases of reduced sediment supply would have allowed for widespread peat formation that ceased at times when mires were overwhelmed by enhanced clastic influx. Such a system was described by Fielding & Webb

(1996) to explain the architecture of the fluvial late Permian Bainmedart coal measures exposed in a corridor-like sub-basin of the Lambert Graben Basin in Antarctica. Fielding & Webb (1996) suggested that peats only formed during phases of minimal sediment supply because neither interfingering of channel and coal deposits nor coal seam splitting were observed. In contrast to a fluvial and mire facies existing side by side, it was concluded that these facies episodically succeeded one another and that these alternations probably reflected the response to precession-scale, orbitally forced climate changes. In the allogenic model of Fielding & Webb (1996), the development of extensive mires, dissected by a network of narrow channels with low clastic loads, is linked to low variations in annual rainfall and high groundwater tables. When seasonality increased, peat formation ceased during the drier months. During the wetter months, discharge was enhanced and a threshold for the confined channel to flood was exceeded, thereby introducing clastic sediment across the mire.

In the fence panel studied here, the interfingering channel sandstones not interrupting the lateral continuity of major coal seams and the time-stratigraphic correlations support episodic allogenic control, *sensu* Fielding & Webb (1996). However, in contrast to a narrow graben basin (Fielding & Webb, 1996), the size of the Western Interior Williston Basin is much larger and, therefore, interfingering channel sandstones interrupting the lateral continuity of major coals outside the study area cannot be ruled out. Nevertheless, it is remarkable that major channel complexes in the Tullock Member seem to occur particularly between major coal seams while there is no field evidence for interruption of the lateral continuity of major coal seams by interfingering major channel sandstones. The mire facies is laterally adjacent to the clastic facies during the transition from the clastic to the mire phase, during enhanced clastic influxes in the mire, and when overlying channels or splays sporadically cut through the peat. However, none of these examples represent interfingering channel sandstones interrupting the lateral continuity of major coal seams. The splitting of major coal seams into minor seams in the Tullock Member differs from the Lambert Graben Basin case, where no clastic partings were observed (Fielding & Webb, 1996). This difference might be related to the linkage with the orbital parameters. Fielding & Webb (1996) linked individual coal seams to precession cycles whereas the major coal seam intervals in the Tullock Member are linked to short-eccentricity cycles. In the Tullock Member, the coal beds split from major coal seams occur on the timescales of precession cycles. However, a possible relation of coal beds and precession cycles would be more complex to prove. The influence of autogenic processes on stacking, at this vertical scale, will increase as well. This is suggested by the higher lateral thickness variation (Fig. 6) of the minor successions with a positive skewed distribution of the histogram (Fig. 7). One example of a potentially relevant autogenic process is the lateral migration of small channels due to a decrease in accommodation rate after compaction of underlying peat (e.g. Van Asselen *et al.*, 2009). Nevertheless, the spectra reveal significant peaks in high-frequency bands that are associated with the minor successions (Fig. 7). These occur in the thickness range where precession forcing would be expected based on the eccentricity scale of the major successions. Further research is needed to explore whether the minor successions could have been controlled by precession cycles and if that control can be disentangled from autogenic processes.

Conceptual models for orbital-scale climate control in the Tullock Member

Taking into account the considerations outlined earlier on, two conceptual models for short-eccentricity-scale climate control on peat formation in the fluvial system of the Tullock Member are described below. The models, dubbed conceptual models 1 and 2, are illustrated in five stages within one 100 kyr eccentricity cycle (Figs 10 and 11).

The main difference between the models is the stratigraphic architecture. Conceptual model 1 is with, and conceptual model 2 is without, interfingering channel sandstones interrupting the lateral continuity of major coal seams. In conceptual model 1, peat formation depends on local autogenic compaction processes that are regionally paced and intensified by orbitally forced climate change. In conceptual model 2, peat formation primarily depends on upstream changes in sediment supply driven by orbitally forced climate changes.

When considering the presence of short-eccentricity climate control, it is important to be aware that the direct influence of eccentricity on annual global insolation, and therefore climate, is very small and that the main influence of eccentricity

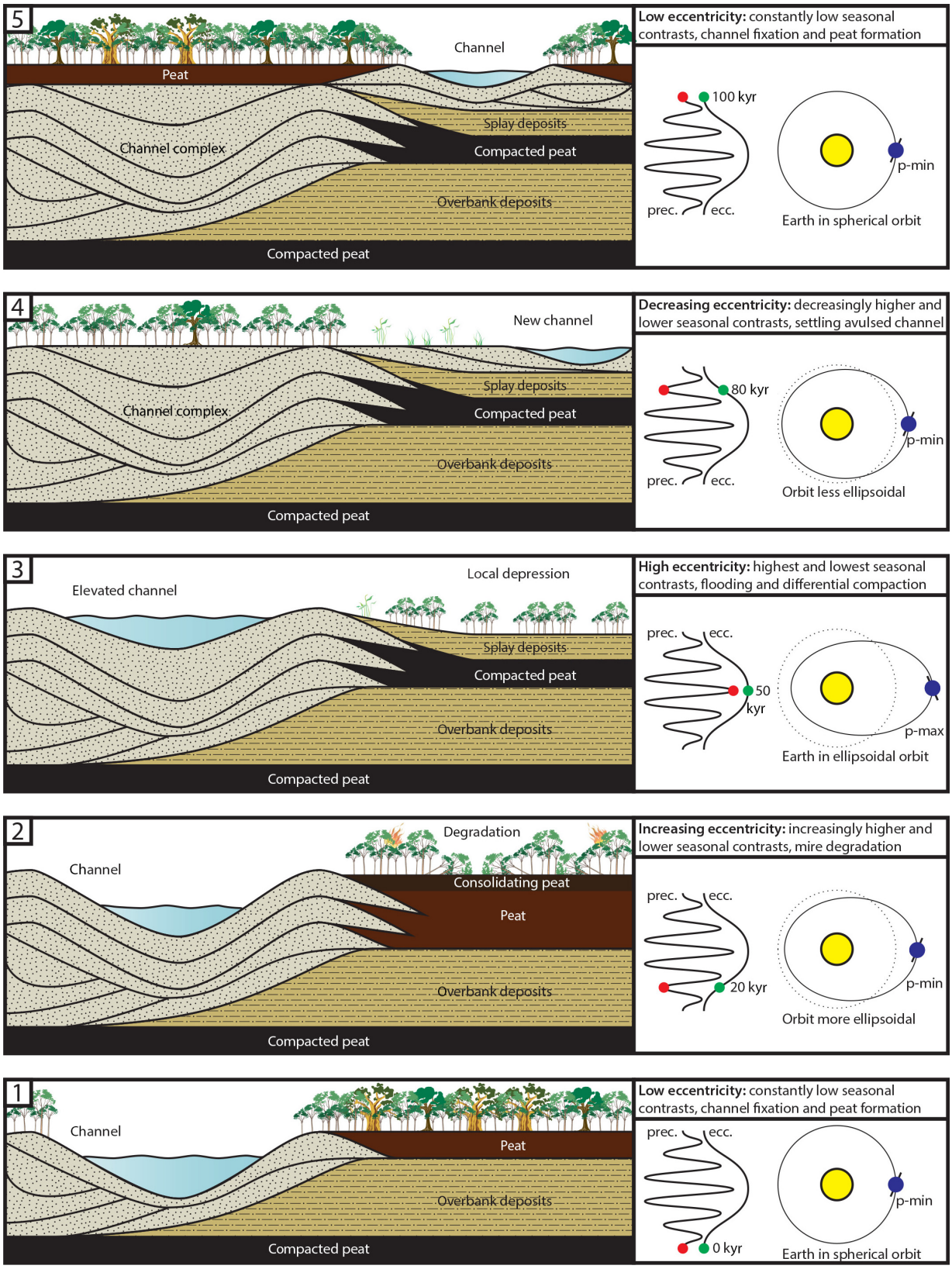

Fig. 10. Conceptual model 1 for short-eccentricity-driven climate control on peat formation in the Tullock Member illustrated in five stages. Timing of peat compaction and autogenic avulsion are controlled by short-eccentricity-scale climate change. A detailed description is provided in the text.

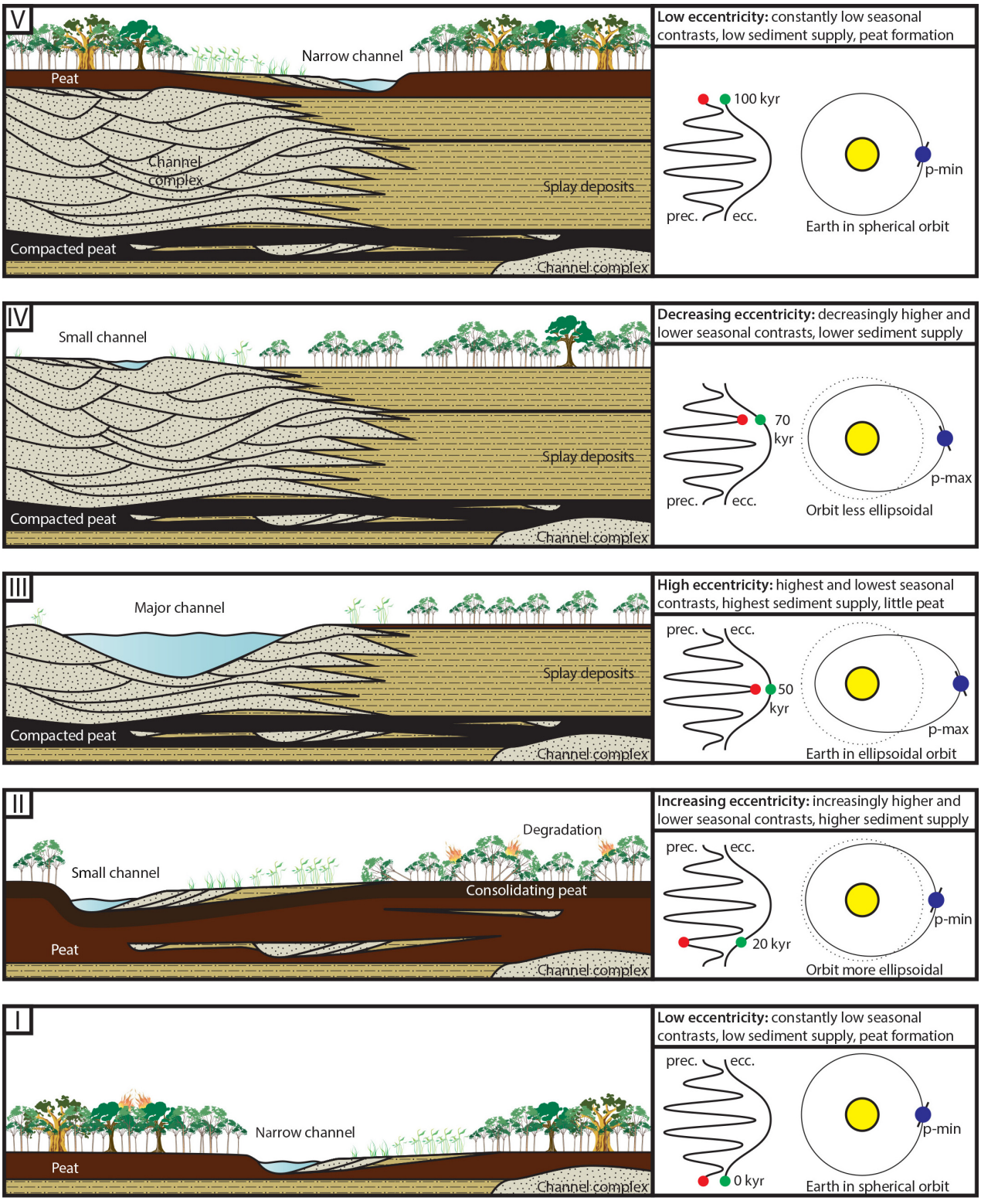

Fig. 11. Conceptual model 2 for short-eccentricity-driven climate control on peat formation in the Tullock Member illustrated in five stages. Upstream changes in sediment supply are controlled by short-eccentricity-scale climate change. A detailed description is provided in the text.

originates from its amplitude modulation of the precession cycle (e.g. Hilgen *et al.*, 2015). Precession, and its control on seasonality and seasonal contrast, has therefore been included in the models to understand the potential eccentricity control on the major phases of peat formation in the fluvial system. In the Northern Hemisphere, highest seasonal contrast occurs at times of minimum precession in combination with high eccentricity. The 41 kyr obliquity cycle mainly influences seasonality at high latitudes but may also have impact at low latitudes during times of low eccentricity without high-latitude ice-sheet fluctuations (Bosmans *et al.*, 2015). The models focus on the scale of major successions linked to the 100 kyr short-eccentricity cycle, which is beyond the timescales of the 41 kyr obliquity cycle and the 20 kyr precession cycle. In contrast to the amplitude modulation of the precession cycle by eccentricity, the effect of eccentricity on the amplitude of the obliquity cycle is minimal. Therefore, obliquity is not included in this model.

Coal petrographic analysis has shown that woody plants were present in the peat-forming area (the inertinite and textinite includes many wood fragments, and ulminite indicates a wet forested peatland). However, the more general term mire is retained in the models below, because it is not known whether or not the area was forested throughout all peat-forming time intervals.

Conceptual model 1 – interfingering of channel and mire facies, timing of peat compaction and avulsion controlled by orbitally forced climate change

Stage 1: Steady climate conditions and prolonged reduced seasonality result in high and stable groundwater levels (Fig. 10). These conditions favour vegetation growth and, in combination with accommodation, result in peat accumulation at relatively fast rates. As a consequence of enhanced peat formation, mires become raised with respect to the channel. Entrenched by vegetation, the channel is depositing coarser-grained sediments mainly within the channel belt while finer-grained material bypasses the area apart from local overbank flooding events. Gradual channel infill results in stacked, cross-bedded sandstone successions interfingering with the adjacent peat layers. Frequency of flooding is low since the raised mire is protected against inundation during increased discharges. Stable floodplain conditions with 'climax' vegetation can be related to phases of low eccentricity when seasonal contrast is reduced for a prolonged period of time (i.e. several precession cycles).

Stage 2: Cyclic increases in seasonality and more prolonged and pronounced periods of drought cause lowering of the groundwater table. Vegetation and peats degrade as result of water deficiency, and mires are decomposed by oxidation leading to peat consolidation. At this time, the decomposed and dehydrated mire loses significant protection against crevasse splaying. Damage to vegetation by wildfires might also increase during prolonged drought and could contribute to the loss of protection. A 'fire splay' (Staub & Cohen, 1979) could result if the peat surface burns but no evidence for that was found in the five *in situ* lignite pillars that have been studied. Meanwhile, the channel becomes super-elevated with respect to the subsiding floodplain since sedimentation in the channel continues. Decreasing floodplain stability during mire degradation can be related to phases of increasing eccentricity when seasonal contrast is periodically enhanced (i.e. at times of minimum precession and stronger Northern Hemisphere summer insolation).

Stage 3: During wet seasons with high seasonal discharge, the river breaks through its levées, leading to floods across the destabilized mire. The peat significantly compacts due to overloading by crevasse splay deposits, increasing the topographic difference between the channel belt and the floodplain. Subsidence in the local flood basin accelerates as a result of peat compaction due to sediment loading. The resulting local topographic depression provides favourable conditions for the channel to avulse in the next stage. Unstable floodplain conditions with the absence of mires can be related to phases of high eccentricity when seasonal contrast is periodically highest (i.e. at times of minimum precession and maximum Northern Hemisphere summer insolation).

Stage 4: An avulsed channel laterally migrates to a topographic low and forms point-bar accretions eroding older overbank deposits. Shortly after deposition, point-bars are colonized by pioneer vegetation which is successively replaced by more established vegetation. Increasingly stable wet conditions cause a raised groundwater table that favours widespread vegetation. Forests colonize the floodplain increasing overbank cohesiveness and causing the channel to aggrade at a relatively fixed position. Increasing floodplain stability, leading to mire development, is related

to periods of decreasing eccentricity (from maximum to minimum values) when high seasonal contrasts are attenuated (i.e. amplitudes of the precession cycle are becoming lower). After this stage, a renewed phase of channel belt aggradation, interfingering with coeval peat formation, continues during periods of reduced seasonal contrast at times of low eccentricity (Stage 5, equivalent to Stage 1).

Conceptual model 2 – fluvial and mire facies succeeded one another, upstream changes in sediment supply controlled by orbitally forced climate change

Stage I: A widespread peat-forming mire develops over an underlying clastic palaeorelief during years with minor change in annual rainfall (Fig. 11). At times of slightly enhanced discharge, a small channel system progrades in the mire, locally causing peat compaction below the channel. When the peat compaction rate decreases, and sedimentation in the channel continues, the channel is subject to decreasing accommodation space and migrates laterally. Damage to vegetation by wildfires, known to be present in the area, may increase the likelihood of small-scale channel avulsion. Widespread mire development and low sediment supply are related to periods of low eccentricity with constantly low seasonal contrast. Relatively stable groundwater levels prevail for a prolonged period of time (one or more precession cycles).

Stage II: At a time of increased seasonal contrast, a prolonged period of drought significantly lowers the groundwater table in the mire causing oxidation of upper peat layers. Regionally, the mire destabilizes due to consolidated peat and becomes more vulnerable to crevasse splaying. Damage to vegetation by wildfires during prolonged drier conditions might also contribute to destabilization of the mire. When discharge and sediment supply increase the channel probably breaks out of its levées, leading to floods across the mire. Peat oxidation leading to mire destabilization during increased seasonal dryness enhances the frequency of crevasse splaying during increased seasonal wetness, which is in turn related to increasing eccentricity when seasonal contrast becomes higher during precession minima.

Stage III: At times of high seasonal discharge and enhanced sediment supply, a major channel develops and frequent flooding forms crevasse splay deposits proximal – and lacustrine splays distal – to the channel. The weight of the overburden on top of the peat causes compaction. Vertical aggradation within the channel belt prevails because there is sufficient accommodation space and avulsion is not triggered by differential compaction since the high frequency of crevasse splaying prevents significant peat formation on the floodplain. Only minor peat develops on the floodplain during episodes of minimal seasonal contrast, but these thin peats are frequently eroded during subsequent crevasse splaying. Enhanced sediment supply and minor peat formation are related to phases of high eccentricity with highest seasonal contrast during the precession minima (enhanced clastic sediment influx) and lowest seasonal contrast during the precession maxima (short-lived peat formation).

Stage IV: During phases of decreased seasonal contrast, sediment supply reduces, decreasing the size of the channel. Because crevasse splay frequencies also decrease, a forest starts to develop over the clastic palaeorelief. Reduced sediment supply and development of a forest during decreased seasonal contrast can be related to decreasing eccentricity when seasonal contrast becomes lower during precession minima. After this stage, a renewed phase dominated by peat formation starts during periods of reduced seasonal contrast at times of lower eccentricity (Stage V, equivalent to Stage I).

Model validation

The most valid model for a specific scale of deposition would be the one capable of reproducing the stratigraphic architecture of that scale. The 10 km wide stratigraphic fence panel that was constructed perpendicular to east/south-east palaeo-flow (Figs 1 and 6) depicts the scale of major sedimentological variation that was the focus of this study. A crucial observation in the fence panel is that interfingering channel sandstones do not interrupt lateral continuity of major coal seams. Major clastic facies and major peat facies may have episodically succeeded one another, comparable to the model of Fielding & Webb (1996). Given the stratigraphic architecture of the fence panel depicting the scale of major successions, conceptual model 1 is considered less optimal for this scale of deposition since the control of peat compaction on channel belt avulsion starts with a channel belt and mire facies existing side by side. As a consequence, interfingering of these facies through time will interrupt the lateral continuity of peat. Conceptual model 2 is

capable of reproducing the stratigraphic architecture in the fence panel, since this model separates a clastic phase dominated by channels and crevasse splays from a succeeding peat-forming phase dominated by mires. Based on these observations, conceptual model 2 is now seen as the most valid model for this scale of deposition.

CONCLUSIONS

Magnetostratigraphic and tephrastratigraphic correlation of thirteen sedimentologically logged sections suggests that eight successive major coal seams are laterally continuous in a *ca* 10 km wide fence panel of the lower Palaeocene Tullock Member. Using ranges of the spectral peaks that represent the average (normally distributed) thickness of major successions in the fence panel, bandpass filtering of high-resolution overbank series reveals a pattern that is regular and similar, especially when the coal seams are decompacted. Evaluation of ages for the C29r/C29n polarity reversal, and $^{40}Ar/^{39}Ar$ radioisotope ages of tephras adjacent to the study area, implies that the timeframe of deposition can be consistent with major peat formation (hence major coal seams) being controlled by 100 kyr orbital eccentricity cycles.

Two conceptual models can explain short-eccentricity-scale climate control on peat formation in the fluvial system. Both models link the major peat-forming phases to low eccentricity. In conceptual model 1, differential peat compaction, leading to river avulsion, is paced during increasing eccentricity at times of minimum precession. High seasonal contrast leads to drying and oxidation, hence compaction, of the peat during the dry season, and enhanced discharges lead to crevasse splaying during the wet season. In conceptual model 2, peat formation depends on short-eccentricity-driven changes in upstream sediment supply with enhanced sediment supply and minor peat formation during high eccentricity, and minor sediment supply and enhanced peat formation during low eccentricity. The fence panel observations, where interfingering channel sandstones do not interrupt the lateral continuity of major coal seams, support conceptual model 2. Splitting of major coal seams into several minor coal seams, over relatively short distances, resulted from phases of increased clastic influx. The horizontal-scale resolution of the fence panel is not sufficient to disentangle autogenic from external forcing, such as precession-scale climate change, in these minor successions.

ACKNOWLEDGEMENTS

Darlyne Dascher and Silvan and Bob Walden are sincerely thanked for providing access to their land. Evelien Rost and Isis van Wetten are acknowledged for their field and laboratory contributions concerning palaeomagnetic sampling and measurements. Maxim Krasnoperov (Utrecht University, NL) assisted in the palaeomagnetic laboratory Fort Hoofddijk. Jim Hower (University of Kentucky, USA) and Neil Holloway (Royal Holloway University of London, UK) prepared the coal petrographic samples. Joep Storms (Delft University of Technology, NL) is thanked for sharing his expertise and for valuable discussions. The article considerably benefited from the thoughtful reviews of, and comments made by, Christopher Fielding, Courtney Sprain, Joan Esterle, Greg Nadon, Peter Warwick, Sian Davies-Vollum and Rhodri Jerrett. This study was made possible by NWO-ALW VIDI grant 864.12.005 to KFK. The authors do not have any conflict of interest.

REFERENCES

Abels, H.A., **Kraus, M.J.** and **Gingerich, P.D.** (2013) Precession-scale cyclicity in the fluvial lower Eocene Willwood Formation of the Bighorn Basin, Wyoming (USA). *Sedimentology*, **60**, 1467–1483.

Aitken, J.F. and **Flint, S.S.** (1995) The application of high-resolution sequence stratigraphy to fluvial systems: a case study from the Upper Carboniferous Breathitt Group, eastern Kentucky, USA. *Sedimentology*, **42**, 3–30.

Alvarez, L.W. (1983) Experimental evidence that an asteroid impact led to the extinction of many species 65 million years ago. *Proc. Natl Acad. Sci. USA*, **80**, 627–642.

Alvarez, L.W., **Alvarez, W.**, **Asaro, F.** and **Michel, H.V.** (1980) Extraterrestrial cause for the Cretaceous-Tertiary extinction. *Science*, **208**, 1095–1108.

Archibald, J.D. (1982) *A study of Mammalia and Geology Across the Cretaceous-Tertiary Boundary in Garfield County*. Univ of California Press, Montana.

Baadsgaard, H., **Lerbekmo, J.** and **McDougall, I.** (1988) A radiometric age for the Cretaceous-Tertiary boundary based upon K-Ar, Rb-Sr, and U-Pb ages of bentonites from Alberta, Saskatchewan, and Montana. *Can. J. Earth Sci.*, **25**, 1088–1097.

Baldwin, B. and **Butler, C.O.** (1985) Compaction curves. *AAPG Bull.*, **69**, 622–626.

Belcher, C.M., **Finch, P.**, **Collinson, M.E.**, **Scott, A.C.** and **Grassineau, N.V.** (2009) Geochemical evidence for

combustion of hydrocarbons during the KT impact event. *Proc. Natl Acad. Sci. USA*, **106**, 4112–4117.

Bohacs, K. and **Suter, J.** (1997) Sequence stratigraphic distribution of coaly rocks: fundamental controls and paralic examples. *AAPG Bull.*, **81**, 1612–1639.

Bohor, B.F., **Foord, E.E.**, **Modreski, P.J.** and **Triplehorn, D.M.** (1984) Mineralogic evidence for an impact event at the Cretaceous-Tertiary boundary. *Science*, **224**, 867–869.

Bosmans, J.H.C., **Hilgen, F.J.**, **Tuenter, E.** and **Lourens, L.J.** (2015) Obliquity forcing of low-latitude climate. *Climate Past*, **11**, 221–241.

Brown, R.W. (1952) Tertiary strata in eastern Montana and western North and South Dakota. Billings Geological Society: Guidebook: Third Annual Field Conference, 89–92.

Cecil, C.B. (1990) Paleoclimate controls on stratigraphic repetition of chemical and siliciclastic rocks. *Geology*, **18**, 533–536.

Cecil, C.B., **DiMichele, W.A.** and **Elrick, S.D.** (2014) Middle and Late Pennsylvanian cyclothems, American Midcontinent: Ice-age environmental changes and terrestrial biotic dynamics. *C.R. Geosci.*, **346**, 159–168.

Chadima, M. and **Hrouda, F.** (2006) Remasoft 3.0 a user-friendly paleomagnetic data browser and analyzer. *Trav. Géophys.*, **27**, 20–21.

Cherven, V.B. and **Jacob, A.F.** (1985) Evolution of Paleogene depositional systems, Williston Basin, in response to global sea level changes. In: *Cenozoic Paleogeography of the West-Central United States* (Eds F.M. Flores and S.S. Kaplan), Rocky Mountain Section (SEPM), 127–170.

Clyde, W.C., **Ramezani, J.**, **Johnson, K.R.**, **Bowring, S.A.** and **Jones, M.M.** (2016) Direct high-precision U–Pb geochronology of the end-Cretaceous extinction and calibration of Paleocene astronomical timescales. *Earth Planet. Sci. Lett.*, **452**, 272–280.

Collier, A.J. and **Knechtel, M.M.** (1939) The coal resources of McCone county. US Geological Survey Bulletin, 905, 80 p. Montana. US Government Printing Office.

Collinson, M.E., **Steart, D.**, **Scott, A.**, **Glasspool, I.** and **Hooker, J.** (2007) Episodic fire, runoff and deposition at the Palaeocene–Eocene boundary. *J. Geol. Soc.*, **164**, 87–97.

Cross, T.A. (1988) Controls on coal distribution in transgressive-regressive cycles, Upper Cretaceous, Western Interior, USA. In: *Sea-Level Changes—An Integrated Approach* (Eds C.K. Wilgus, B.S. Hastings, C.G.St.C. Kendall, H.W. Posamentier, C.A. Ross and J.C. Van Wagoner), SEPM Special Publication, **42**, 371–380.

Davies-Vollum, K.S. and **Smith, N.D.** (2008) Factors affecting the accumulation of organic-rich deposits in a modern avulsive floodplain: examples from the Cumberland Marshes, Saskatchewan, Canada. *J. Sed. Res.*, **78**, 683–692.

DeCelles, P.G. (2004) Late Jurassic to Eocene evolution of the Cordilleran thrust belt and foreland basin system, western USA. *Am. J. Sci.*, **304**, 105–168.

Diessel, C.F.K. (1992) Coal formation and sequence stratigraphy. In: *Coal-Bearing Depositional Systems* (Ed. C.F.K. Diessel), pp. 461–514. Springer, Berlin.

Erickson, J.M. (1999) The Dakota Isthmus – Closing the Late Cretaceous Western Interior Seaway. *Proc. North Dakota Acad. Sci.*, **53**, 124–129.

Fastovsky, D.E. (1987) Paleoenvironments of vertebrate-bearing strata during the Cretaceous-Paleogene transition, eastern Montana and western North Dakota (USA). *Palaios*, **2**, 282–295.

Fastovsky, D.E. and **Bercovici, A.** (2016) The Hell Creek Formation and its contribution to the Cretaceous-Paleogene extinction: A short primer. *Cretaceous Res.*, **57**, 368–390.

Fastovsky, D.E. and **Dott Jr, R.H.** (1986) Sedimentology, stratigraphy, and extinctions during the Cretaceous-Paleogene transition at Bug Creek, Montana (USA). *Geology*, **14**, 279–282.

Fielding, C. (1984) A coal depositional model for the Durham Coal Measures of NE England. *J. Geol. Soc.*, **141**, 919–931.

Fielding, C.R. and **Webb, J.A.** (1996) Facies and cyclicity of the Late Permian Bainmedart Coal Measures in the Northern Prince Charles Mountains, MacRobertson Land, Antarctica. *Sedimentology*, **43**, 295–322.

Fisher, R. (1953) Dispersion on a sphere. *Proc. Roy. Soc. London A Math. Phys. Eng. Sci.*, **217**, 295–305.

Flores, R. and **Keighin, C.** (1999) Fort Union coal in the Williston Basin, North Dakota: a synthesis. *US Geol. Surv. Prof. Pap. A*, **1625**, 1–45.

Flores, R., **Keighin, C.**, **Ochs, A.**, **Warwick, P.**, **Bader, L.** and **Murphy, E.** (1999) Framework geology of Fort Union coal in the Williston Basin. *Fort Union Assessment Team US Geol. Surv. Prof. Pap.*, **1625-A**, 1–64.

Glasspool, I.J. and **Scott, A.C.** (2010) Phanerozoic concentrations of atmospheric oxygen reconstructed from sedimentary charcoal. *Nature Geosci.*, **3**, 627–630.

Hartman, J.H., **Butler, R.D.**, **Weiler, M.W.** and **Schumaker, K.K.** (2014) Context, naming, and formal designation of the Cretaceous Hell Creek Formation lectostratotype, Garfield County, Montana. *Geol. Soc. Am. Spec. Pap.*, **503**, 89–121.

Heckel, P.H. (2008) Pennsylvanian cyclothems in Midcontinent North America as far-field effects of waxing and waning of Gondwana ice sheets. *Geol. Soc. Am. Spec. Pap.*, **441**, 275–289.

Hilgen, F.J., **Hinnov, L.A.**, **Aziz, H.A.**, **Abels, H.A.**, **Batenburg, S.**, **Bosmans, J.H.**, **de Boer, B.**, **Hüsing, S.K.**, **Kuiper, K.F.** and **Lourens, L.J.** (2015) Stratigraphic continuity and fragmentary sedimentation: the success of cyclostratigraphy as part of integrated stratigraphy. *Geol. Soc. London. Spec. Publ.*, **404**, 157–197.

ICCP (1963) *International Committee for Coal Petrology. International Handbook for Coal Petrography*. Centre National De La Recherche Scientifique, France.

ICCP (2001) International Committee for Coal Petrology. The new inertinite classification (ICCP System 1994). *Fuel*, **80**, 459–471.

Ickert, R.B., **Mulcahy, S.R.**, **Sprain, C.J.**, **Banaszak, J.F.** and **Renne, P.R.** (2015) Chemical and Pb isotope composition of phenocrysts from bentonites constrains the chronostratigraphy around the Cretaceous-Paleogene boundary in the Hell Creek region, Montana. *Geochem. Geophys. Geosyst.*, **16**, 2743–2761.

Jerrett, R.M., **Price, G.D.**, **Grimes, S.T.** and **Dawson, A.T.** (2015) A paleoclimatic and paleoatmospheric record from peatlands accumulating during the Cretaceous-Paleogene boundary event, Western Interior Basin, Canada. *Geol. Soc. Am. Bull.*, **127**, 1564–1582.

Kirschvink, J. (1980) The least-squares line and plane and the analysis of palaeomagnetic data. *Geophys. J. Int.*, **62**, 699–718.

LeCain, R., **Clyde, W.C.**, **Wilson, G.P.** and **Riedel, J.** (2014) Magnetostratigraphy of the Hell Creek and lower fort union formations in northeastern Montana. *Geol. Soc. Am. Spec. Pap.*, **503**, 137–147.

Lofgren, D.L. (1995) The Bug Creek problem and the Cretaceous-Tertiary transition at McGuire Creek, Montana. *Univ. Calif. Publ. Geol. Sci.*, **140**, 185.

Lofgren, D.L., **Hotton, C.L.** and **Runkel, A.C.** (1990) Reworking of Cretaceous dinosaurs into Paleocene channel, deposits, upper Hell Creek Formation, Montana. *Geology*, **18**, 874–877.

Michaelsen, P. and **Henderson, R.A.** (2000) Facies relationships and cyclicity of high-latitude, Late Permian coal measures, Bowen Basin, Australia. *Int. J. Coal Geol.*, **44**, 19–48.

Moore, J.R., **Wilson, G.P.**, **Sharma, M.**, **Hallock, H.R.**, **Braman, D.R.** and **Renne, P.R.** (2014) Assessing the relationships of the Hell Creek-Fort Union contact, Cretaceous-Paleogene boundary, and Chicxulub impact ejecta horizon at the Hell Creek Formation lectostratotype, Montana, USA. *Geol. Soc. Am. Spec. Pap.*, **503**, 123–135.

Mullender, T.A.T., **Frederichs, T.**, **Hilgenfeldt, C.**, **de Groot, L.V.**, **Fabian, K.** and **Dekkers, M.J.** (2016) Automated paleomagnetic and rock magnetic data acquisition with an in-line horizontal "2G" system. *Geochem. Geophys. Geosyst.*, **17**, 1–14.

Nadon, G. and **Issler, D.** (1997) The compaction of floodplain sediments: timing, magnitude and implications. *Geosci. Can.*, **24**, 37–43.

Nagata, T., **Akimoto, S.** and **Uyeda, S.** (1951) Reverse thermo-remanent magnetism. *Proc. Jpn. Acad.*, **27**, 643–645.

Paillard, D., **Labeyrie, L.** and **Yiou, P.** (1996) Macintosh program performs time-series analysis. *EOS Trans. Am. Geophys. Union*, **77**, 379.

Paproth, E., **Dusar, M.**, **Verkaeren, P.** and **Bless, M.J.** (1996). Stratigraphy and cyclic nature of lower Westphalian deposits in the boreholes KB174 and KB206 in the Belgian Campine. Annales de la Société géologique de Belgique.

Peppe, D., **Evans, D.** and **Smirnov, A.** (2009) Magnetostratigraphy of the Ludlow Member of the Fort Union Formation (Lower Paleocene) in the Williston Basin, North Dakota. *Geol. Soc. Am. Bull.*, **121**, 65–79.

Renne, P.R., **Deino, A.L.**, **Hilgen, F.J.**, **Kuiper, K.F.**, **Mark, D.F.**, **Mitchell 3rd, W.S.**, **Morgan, L.E.**, **Mundil, R.** and **Smit, J.** (2013) Time scales of critical events around the Cretaceous-Paleogene boundary. *Science*, **339**, 684–687.

Retallack, G.J. (1994) A pedotype approach to latest Cretaceous and earliest Tertiary paleosols in eastern Montana. *Geol. Soc. Am. Bull.*, **106**, 1377–1397.

Rigby, J. and **Rigby Jr, J.** (1990) Geology of the sand arroyo and bug creek quadrangles. *McCone County Montana Brigham Young Univ. Geol. Stud.*, **36**, 69–134.

Rigby Jr, J.K., **Newman, K.R.**, **Van Der Kaars, J.S.S.**, **Sloan, R.E.** and **Rigby, J.K.** (1987) Dinosaurs from the Paleocene part of the Hell Creek Formation, McCone County, Montana. *Palaios*, **2**, 296–302.

Robson, B.E., **Collinson, M.E.**, **Riegel, W.**, **Wilde, V.**, **Scott, A.C.** and **Pancost, R.D.** (2015) Early Paleogene wildfires in peat-forming environments at Schöningen, Germany. *Palaeogeogr. Palaeoclimatol. Palaeoecol.*, **437**, 53–62.

Schulz, M. and **Mudelsee, M.** (2002) REDFIT: estimating red-noise spectra directly from unevenly spaced paleoclimatic time series. *Compute. Geosci.*, **28**, 421–426.

Sclater, J.G. and **Christie, P.** (1980) Continental stretching; an explanation of the post-Mid-Cretaceous subsidence of the central North Sea basin. *J. Geophys. Res.*, **85**, 3711–3739.

Scott, A.C. (2010) Charcoal recognition, taphonomy and uses in palaeoenvironmental analysis. *Palaeogeogr. Palaeoclimatol. Palaeoecol.*, **291**, 11–39.

Scott, A.C. and **Glasspool, I.J.** (2007) Observations and experiments on the origin and formation of inertinite group macerals. *Int. J. Coal Geol.*, **70**, 53–66.

Sloan, R.E. and **Rigby Jr, J.K.** (1986) Response: Cretaceous-Tertiary dinosaur extinction. *Science*, **234**, 1173–1175.

Sloan, R.E. and **Van Valen, L.** (1965) Cretaceous mammals from Montana. *Science*, **148**, 220–227.

Sloan, R.E., **Rigby Jr, J.K.**, **Van Valen, L.M.** and **Gabriel, D.** (1986) Gradual dinosaur extinction and simultaneous ungulate radiation in the Hell Creek Formation. *Science*, **232**, 629–633.

Smit, J. and **Hertogen, J.** (1980) An extraterrestrial event at the Cretaceous-Tertiary boundary. *Nature*, **285**, 198–200.

Smit, J. and **Klaver, G.** (1981) Sanidine spherules at the Cretaceous-Tertiary boundary indicate a large impact event. *Nature*, **292**, 47–49.

Smit, J. and **van der Kaars, S.** (1984) Terminal Cretaceous extinctions in the Hell Creek area, Montana: compatible with catastrophic extinction. *Science*, **223**, 1177–1179.

Smit, J., **van der Kaars, S.** and **Rigby Jr, J.K.** (1987) Stratigraphic aspects of the Cretaceous-Tertiary boundary in the Bug Creek area of eastern Montana, USA. *Mém. de la Soc. Geol. de France Nouvelle Sérié*, **150**, 53–73.

Sprain, C.J., **Renne, P.R.**, **Wilson, G.P.** and **Clemens, W.A.** (2015) High-resolution chronostratigraphy of the terrestrial Cretaceous-Paleogene transition and recovery interval in the Hell Creek region, Montana. *Geol. Soc. Am. Bull.*, **127**, 393–409.

Sprain, C.J., **Feinberg, J.M.**, **Renne, P.R.** and **Jackson, M.** (2016) Importance of titanohematite in detrital remanent magnetizations of strata spanning the Cretaceous-Paleogene boundary, Hell Creek region, Montana. *Geochem. Geophys. Geosyst.*, **17**, 660–678.

Staub, J.R. and **Cohen, A.D.** (1979) The Snuggedy Swamp of South Carolina: a back-barrier estuarine coal-forming environment. *J. Sed. Res.*, **49**, 133–143.

Swisher III, C.C., **Dingus, L.** and **Butler, R.F.** (1993) 40Ar/39Ar dating and magnetostratigraphic correlation of the terrestrial Cretaceous-Paleogene boundary and Puercan Mammal Age, Hell Creek-Tullock formations, eastern Montana. *Can. J. Earth Sci.*, **30**, 1981–1996.

Sýkorová, I., **Pickel, W.**, **Christanis, K.**, **Wolf, M.**, **Taylor, G.** and **Flores, D.** (2005) Classification of huminite—ICCP System 1994. *Int. J. Coal Geol.*, **62**, 85–106.

Teichmüller, M. (1989) The genesis of coal from the viewpoint of coal petrology. *Int. J. Coal Geol.*, **12**, 1–87.

Thom, W. and **Dobbin, C.** (1924) Stratigraphy of Cretaceous-Eocene transition beds in eastern Montana and the Dakotas. *Geol. Soc. Am. Bull.*, **35**, 481–506.

Ting, F.T. (1972) Petrified peat from a Paleocene lignite in North Dakota. *Science*, **177**, 165–166.

Ting, F. (1977) Microscopical investigation of the transformation (diagenesis) from peat to lignite. *J. Microsc.*, **109**, 75–83.

Van Asselen, S., **Stouthamer, E.** and **Van Asch, T.W.** (2009) Effects of peat compaction on delta evolution: a review on processes, responses, measuring and modeling. *Earth-Sci. Rev.*, **92**, 35–51.

Vandenberghe, N., **Hilgen, F.J.** and **Speijer, R.** (2012) The paleogene period. In: *The Geologic Time Scale 2012* (Eds

F.M. Gradstein, J.G. Ogg, M. Schmitz and G. Ogg), pp. 855–921. Elsevier, Amsterdam.

Wanless, H.R. and **Weller, J.M.** (1932) Correlation and extent of Pennsylvanian cyclothems. *Geol. Soc. Am. Bull.*, **43**, 1003–1016.

Woolsey, L.H., **Richards, R.W.** and **Lupton, C.T.** (1917) *The Bull Mountain Coal Field, US Geological Survey Bulletin*, **647**. US Government Printing Office, Musselshell and Yellowstone Counties, Montana, 218 pp.

Zachos, J.C., **McCarren, H.**, **Murphy, B.**, **Röhl, U.** and **Westerhold, T.** (2010) Tempo and scale of late Paleocene and early Eocene carbon isotope cycles: implications for the origin of hyperthermals. *Earth Planet. Sci. Lett.*, **299**, 242–249.

Zijderveld, J. (1967) AC demagnetization of rocks: analysis of results. *Meth. Paleomagnetism*, **3**, 254–286.

Manuscript received 30 September 2016; revision accepted 21 July 2017

Supporting Information

Additional Supporting Information may be found in the online version of this article:

Figure S1. Detailed sedimentological logs of the six composite sections of Rock Creek Main (RCM), Rock Creek East (RCE), Purgatory Hill Main (PHM), Purgatory Hill South-east (PHSE), Bug Creek Main (BCM) and Bug Creek South-east (BCSE).

Figure S2. Magnetic polarity plots of Rock Creek East (S2A), Purgatory Hill Main (S2B), Purgatory Hill South-east (S2C), Bug Creek Main (S2D), and Bug Creek South-east (S2E).

Figure S3. Plate of microscope images from polished blocks of lignite taken in reflected light (A) to (E) and reflected fluorescent light (F).

Figure S4. Upper left part*:* REDFIT spectral analysis of the coal decompacted GSI record of BOC. Peaks show higher significance after the decompaction. Filter range of the most significant spectral peak at *ca* 3.5 m is indicated. Spectral power at *ca* 8 m is also present but less significant. Right part: Bandpass Gaussian filter of the *ca* 3.5 m peak. The filter tends to trace some of the coal splits, such as in coals #1-Z, #3-Y and #4-X, but probably primarily originates from an overlap in frequencies between minor and major successions.

Appendix S1. Supplementary information on field methods and sampling, coal macerals and re-sampling of grain size index (GSI) data and settings in REDFIT spectral analysis.

Appendix S2. Magnetostratigraphic data of thermally demagnetized samples.

Appendix S3. Magnetostratigraphic data of samples demagnetized with an alternating field.

Appendix S4. Percentage data of the macerals that were quantified from the huminite, inertinite and liptinite group macerals.

Data S1. Raw palaeomagnetic data of thermally demagnetized (TH) samples.

Data S2. Raw palaeomagnetic data of samples demagnetized with an alternating field (AF).